THE GEOLOGICAL SOCIETY OF AMERICA®

Subduction initiation of the western Paleo-Asian Ocean linked to global tectonic reorganization: Insights from Cambrian island-arc magmatism within the West Junggar, NW China

Yunying Zhang[1,2,3], Min Sun[3], Jiyuan Yin[4,†], Chao Yuan[5], Zhen Sun[1,2], and Xiaoping Xia[5]

[1]*Key Laboratory of Ocean and Marginal Sea Geology, South China Sea Institute of Oceanology, Innovation Academy of South China Sea Ecology and Environmental Engineering, Chinese Academy of Sciences, Guangzhou 510301, China*

[2]*Southern Marine Science and Engineering Guangdong Laboratory, Guangzhou 511458, China*

[3]*Department of Earth Sciences, The University of Hong Kong, Pokfulam Road, Hong Kong, China*

[4]*Key Laboratory of Deep-Earth Dynamics of Ministry of Natural Resources, Institute of Geology, Chinese Academy of Geological Sciences, Beijing 100037, China*

[5]*State Key Laboratory of Isotope Geochemistry, Guangzhou Institute of Geochemistry, Chinese Academy of Sciences, Guangzhou 510640, China*

ABSTRACT

The subduction initiation associated with the beginning of accretionary orogens has been thought to be related to global plate reorganization. To characterize the initial subduction within the western Central Asian Orogenic Belt, this integrated study focuses on Cambrian tholeiitic to calc-alkaline plutons in the Barleik-Mayile-Saleinuohai area of West Junggar, NW China. Zircon U-Pb results of felsic plutons reveal a wide range (511–488 Ma) of ages with older ages up to 514–511 Ma. The felsic rocks exhibit variable SiO_2 (53.0–77.4 wt%) and K_2O (0.05–2.24 wt%) contents and can be classified as diorite, granodiorite, trondhjemite, and tonalite. On the basis of their low TiO_2 (0.12–0.71 wt%) contents and characteristic trace element trends as well as high zircon εHf(t) (+10.5 to +14.5) and mantle-like zircon $\delta^{18}O$ (5.0 ± 0.48‰ to 5.4 ± 0.43‰, two standard deviations) values, we interpret that the Cambrian felsic rocks have diverse origins, involving differentiation of arc basalts and partial melting of subducted oceanic crust, arc mafic crust, and metasomatized mantle wedge. The Saleinuohai gabbroic pluton shows zircon $\delta^{18}O$ ratios from 4.2 to 4.7‰, which are lower than those of igneous zircons in equilibrium with mantle and thus reflect modification of their mantle source by hydrothermal fluids with seawater-like oxygen isotopes at high temperature. Combined with regional data, we propose that the West Junggar arc represents the extending of the Boshchekul-Chingiz arc in the Early Cambrian, defining a long (>1000 km) E-W–trending subduction zone. The earliest island-arc tholeiitic felsic plutons in the West Junggar took place at ca. 514–511 Ma, which, coupled with other early subduction records (e.g., 530 Ma SSZ-type Kopu-relisay ophiolites) in the western Paleo-Asian Ocean, indicates that initial stages of subduction of the western Paleo-Asian Ocean probably occurred in the Early Cambrian. The simultaneity between the initial subduction of the western Paleo-Asian Ocean, Gondwana assembly, and Laurasia breakup suggests a causal link between the three, collectively correlated to a global plate adjustment event.

INTRODUCTION

Subduction zones exert a vital role in shaping the modern Earth system through material exchange (e.g., H_2O and CO_2) between the earth's surface and interior, which influence the surface environment and control natural mineral resources and hazards (Stern, 2002; Kessel et al., 2005; Kelemen and Manning, 2015). Understanding how and when new subduction zones initiate is the prerequisite to further probe global geochemical cycles and plate tectonics over the Earth's history. Based on geological records and numerical models, it is revealed that the start of a new subduction zone is generally attributed to either induced or spontaneous nucleation (Stern, 2004; Stern and Gerya, 2018). The former scenario occurs if gravitational instability grows during regional forcing across a pre-existing weak zone, while the latter is driven by a lateral density contrast between adjacent plates (Stern and Gerya, 2018). On a larger scale, the driving mechanism of subduction initiation associated with accretionary orogens is usually related to global plate kinematic adjustments, such as supercontinent assembly (Cawood and Buchan, 2007). A sequence of well-documented rock records (i.e., fore-arc basalt, boninite, and island-arc tholeiite) that are developed in the modern Izu–Bonin–Mariana subduction zone have been considered as diagnostic petrological markers of subduction initiation (Ishizuka et al., 2014; Arculus et al., 2015), while suprasubduction zone (SSZ) ophiolites in accretionary orogens are comparable with those in the Izu–Bonin–Mariana forearc and thus could provide crucial constraints on understanding how subduction began in ancient intra-oceanic subduction systems (Reagan et al., 2010; Whattam and Stern, 2011).

The Central Asian Orogenic Belt, located between the North China and Tarim cratons to the south and the Siberian Craton to the north (Fig. 1A), represents one of the largest accretionary orogens on Earth (Şengör et al., 1993; Xiao et al., 2015). It is an immense and complex collage of island arc-back arc systems, ophiolitic remnants, accretionary wedges, and microcontinents, and has undergone a long-period (Neoproterozoic to Mesozoic) of subduction-accretionary processes including the birth and demise of the Paleo-Asian Ocean (Windley et al., 2007;

Jiyuan Yin https://orcid.org/0000-0003-3554-7674
[†]Corresponding author: yinjiyuan1983@163.com.

GSA Bulletin;
published online 24 March 2022

https://doi.org/10.1130/B36304.1; 8 figures; 1 supplemental file.

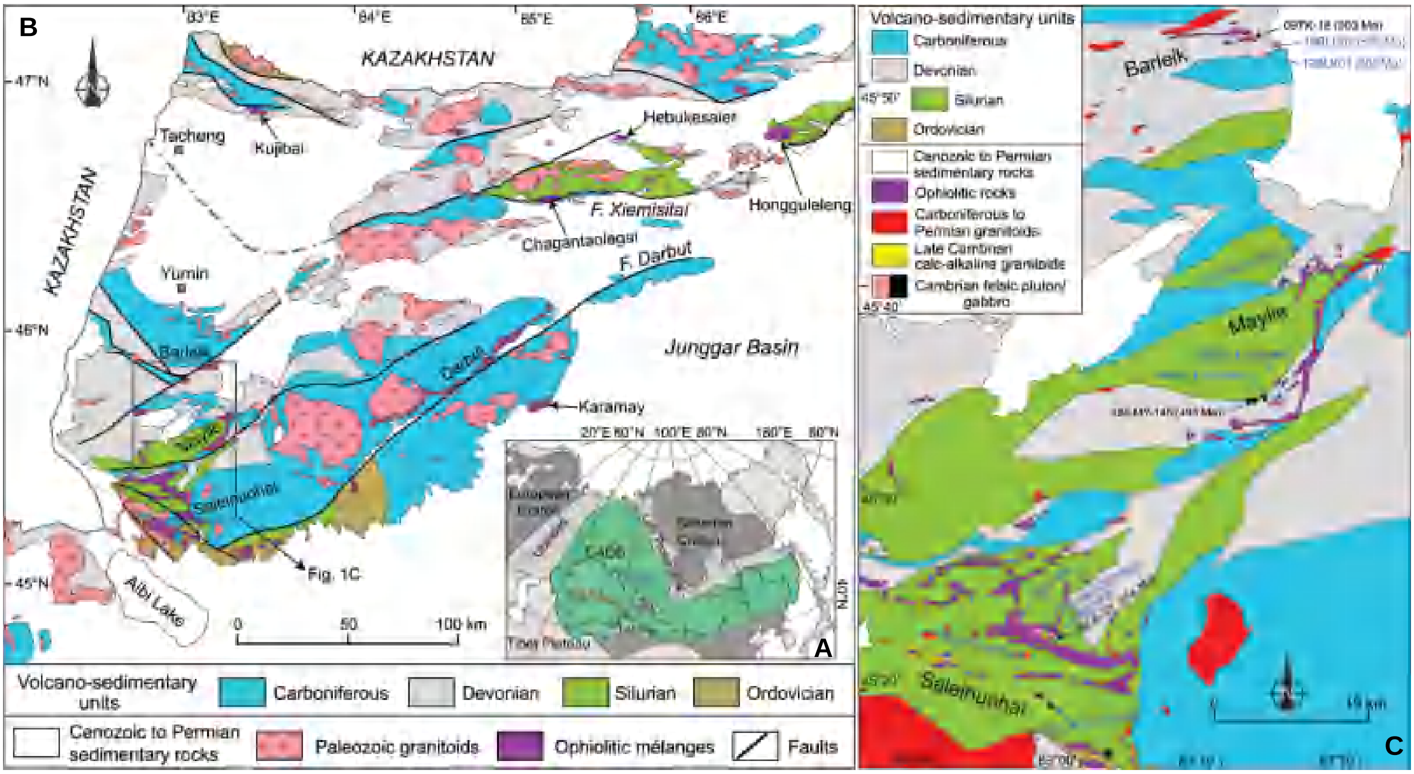

Figure 1. (A) Simplified tectonic map of the Central Asian Orogenic Belt (modified after Jahn et al., 2000). (B) Sketch map of the West Junggar, NW China (modified after Ren et al., 2014). (C) Geological map of the Barleik-Mayile-Saleinuohai area, West Junggar (after Xu et al., 2012, 2013; Ren et al., 2014; Zhang et al., 2018a) showing the distribution of ophiolitic rocks and the localities where felsic and gabbroic plutons were sampled. The black sample labels indicate age results from previous studies (Xu et al., 2012, 2013; Ren et al., 2014), while the blue sample labels show the age results of this study.

Wilhem et al., 2012; Zhang et al., 2018b). Recent provenance, paleomagnetic, and isotopic dating studies from southern Siberia indicate that the opening of the Paleo-Asian Ocean probably commenced at mid-Neoproterozoic time (ca. 760 Ma), due to the breakup of Rodinia that was induced by subduction processes along its periphery (Cawood et al., 2016; Ernst et al., 2016; Zhao et al., 2018). It is recognized that initiation of Mariana-type oceanic subduction in the northern Paleo-Asian Ocean occurred at Neoproterozoic and created the Tuva-Sayan oceanic arc systems around southern Siberia, which was probably correlated to the northward drift of the Siberian Craton and consequent expansion of the Paleo-Asian Ocean (Kuzmichev et al., 2005; Safonova et al., 2017; Wan et al., 2018). In contrast, initial subduction of the southern Paleo-Asian Ocean was much younger (Safonova et al., 2017) and the related driving mechanism in a global setting remains unclear. The West Junggar of NW China occupies the western segment of the southern Central Asian Orogenic Belt and features Cambrian SSZ-type ophiolitic mélanges and related intrusions, probably formed during the initial stages of subduction (Ren et al., 2014; Liu et al., 2016). In this contribution, we conducted whole-rock geochemical and zircon U-Pb-Hf-O isotopic analyses of the Cambrian mafic to felsic plutons that were concomitant with the Barleik-Mayile-Saleinuohai ophiolitic mélanges of West Junggar, aiming to (1) ascertain their timing and petrogenesis and (2) constrain the driving mechanism of the initial subduction of the western Paleo-Asian Ocean in a global context. Combined with previously published data, it is interpreted that the initial subduction of the western Paleo-Asian Ocean was associated with Gondwana assembly and Laurasia breakup.

GEOLOGICAL BACKGROUND AND SAMPLING

Geological Background

The West Junggar, bordered by the Altai range to the north and the Tianshan belt to the south (Fig. 1A), represents a Paleozoic intra-oceanic subduction-accretion system composed of island arcs, seamounts, accretionary complexes, and ophiolitic mélanges (Windley et al., 2007; Xiao and Santosh, 2014). High and positive Nd-Hf isotopic values (εNd(t) = +5.2 to +8.4; zircon εHf(t) = +10.6 to +16.2) of mafic to felsic rocks in the West Junggar strongly support its intra-oceanic arc attribute (Chen and Arakawa, 2005; Geng et al., 2009; Ma et al., 2012; Yin et al., 2013; Chen et al., 2015; Tang et al., 2019). Tectonically, the West Junggar can be divided into the northern and southern parts separated by the Xiemisitai fault (Fig. 1B). The northern West Junggar is made up of two middle to late Paleozoic E-W–trending island arcs with the Hongguleleng-Kujibai ophiolitic mélange in between. This is in contrast to the southern West Junggar where the magmatic arcs and faults are mainly NE-SW oriented (Choulet et al., 2012; Zhang et al., 2018a). Outcropping in the SW region of the southern West Junggar and representing the oldest ophiolitic mélange in the West Junggar, the Barleik-Mayile-Saleinuohai ophiolitic rocks display characteristic "block-in-matrix" structures and are surrounded by arc accretionary complexes (Fig. 1C; Ren et al., 2014; Zhang et al., 2018a). In addition, these ophiolitic rocks show typical SSZ-type geochemical compositions (e.g., spinel and clinopyroxene has high Cr# > 0.6 and Mg# > 90, respectively), suggesting that they were formed in a subduction-related setting (Xu et al., 2012, 2013; Liu et al., 2016).

The Barleik ophiolitic mélange is featured by dispersed blocks in a serpentinite matrix, including peridotite, wehrlite, clinopyroxenite, cumulate gabbro, pillow lava, garnet amphibolite, and blueschist (Xu et al., 2013; Liu et al., 2016). Felsic plutons in this mélange yielded zircon U-Pb ages of 509–503 Ma (Xu et al., 2013). Moreover, phengite and zircon crystals from the blueschist gave an $^{40}Ar/^{36}Ar$ age of 492 ± 4 Ma and a U-Pb age of 502 ± 2 Ma, respectively, and amphibole and rutile grains from the amphibolite gave an $^{40}Ar/^{36}Ar$ age of 504 Ma and a U-Pb age of 502 ± 25 Ma, respectively (Liu et al., 2016). The Mayile and Saleinuohai ophiolitic blocks, mainly consisting of lherzolite, dunite, harzburgite, wehrlite, gabbro, and basalt, are enclosed in Early Silurian turbidites and juxtaposed with Middle-Late Silurian volcanic-sedimentary strata (Bai et al., 1995; Buckman and Aitchison, 2001). In the Mayile ophiolitic mélange, the gabbroic and felsic intrusions yielded zircon U-Pb ages of ca. 493 Ma and 501–485 Ma, respectively (Xu et al., 2012), while in the Saleinuohai ophiolitic mélange, the gabbroic ophiolitic blocks and felsic intrusions yielded zircon U-Pb ages of ca. 516 Ma and 515–509 Ma, respectively (Ren et al., 2014). Although the ages of the Barleik-Mayile-Saleinuohai ophiolitic mélanges are generally understood and the mafic plutons are regarded as melting products of subduction-modified mantle, the petrogenesis of felsic plutons as well as their implications for the initial subduction of the western Paleo-Asian Ocean remains unclear.

Sample Descriptions

The felsic plutons in the Barleik ophiolitic mélange range in composition from dioritic to granodioritic. The diorite pluton is dark green and shows a medium-grained (2–5 mm) massive texture (Fig. 2A), with mineral assemblages of plagioclase (~60 vol%), amphibole (~25 vol%), and quartz (~5 vol%) and minor apatite and zircon, while the granodiorite pluton is off-white (Fig. 2B), shows a fine-grained (1–2.5 mm) massive texture, and consists of plagioclase (45–50 vol%), amphibole (5–10 vol%), K-feldspar (5–10 vol%), quartz (20–25 vol%), and biotite (~5 vol%) (Fig. 2C). The felsic plutons in the Mayile ophiolitic mélange are mainly fine-grained (0.2–1.5 mm) diorites, made up of plagioclase (~60 vol%), amphibole (~30 vol%), and quartz (<5 vol%), with minor apatite and titanite (Fig. 2D). Plagioclase and amphibole occur as subhedral prisms, whereas quartz occurs as anhedral interstitial grains. The felsic plutons in the Saleinuohai ophiolitic mélange are predominantly fine-grained (0.2–2.0 mm) trondhjemite, composed of plagioclase (55–60 vol%) and quartz (30–35 vol%) with subordinate K-feldspar (~2 vol%), zircon, and apatite (Fig. 2E). One gabbroic pluton was also sampled from the Saleinuohai ophiolitic mélange. Minerals of this gabbroic pluton contain plagioclase (50–60 vol%) and pyroxene (30–40 vol%), with minor opaque minerals (Fig. 2F).

ANALYTICAL METHODS

Whole-Rock Major and Trace Elements

Whole-rock major and trace element compositions were measured at the ALS Chemex Co. Ltd. (Guangzhou, China). Major oxides were analyzed using an X-ray fluorescence spectrometer (PANalytical, PW2424, Netherlands) on fused glass disks, with analytical precision better than 4% based on the measurement of Chinese rock standard GBW07105. Trace elements, including large ion lithophile elements (LILE), high field strength elements (HFSE), and rare earth elements (REE), were determined by an

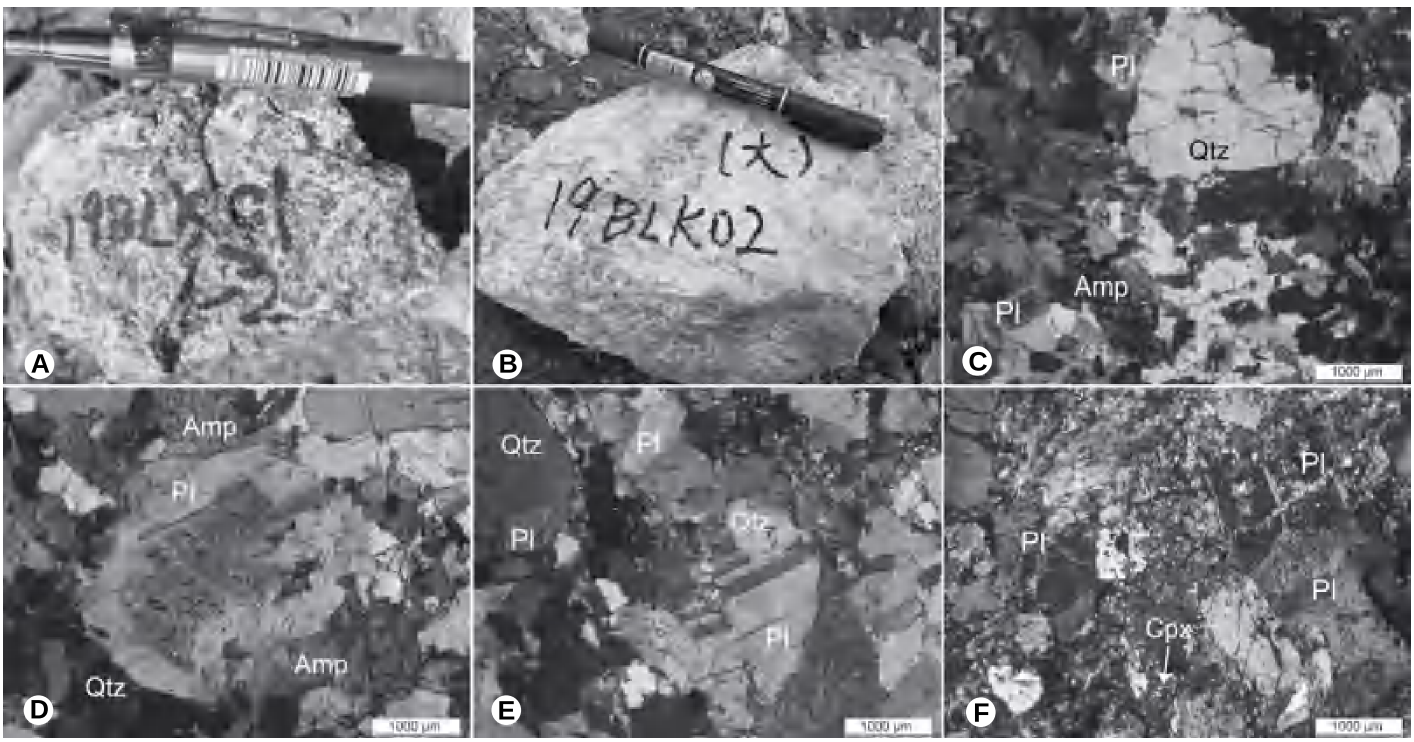

Figure 2. Photographs of outcrops and photomicrographs showing the geological and mineralogical characteristics of the felsic and mafic plutons from the Barleik-Mayile-Saleinuohai (BMS) ophiolitic mélanges of the West Junggar, NW China. The diorite (A) and granodiorite (B–C) plutons from the Barleik ophiolitic mélange. The diorite pluton (D) from the Mayile ophiolitic mélange. The trondhjemite (E) and gabbro (F) plutons from the Saleinuohai ophiolitic mélange. Pl—plagioclase; Qtz—quartz; Cpx—clinopyroxene; Amp—amphibole.

Agilent 7900 inductively coupled plasma–mass spectrometer (ICP-MS) equipment and a Varian ICP745-ES inductively coupled plasma–atomic emission spectrometry (ICP-AES) instrument. Rock powders (~50 mg) were digested using $HF + HNO_3 + HClO_4$ acid mixture and then the solutions were analyzed. The standards MRGeo08, OREAS-120, OREAS-460, and OREAS-100a were run as unknowns to monitor the data quality, the precision was generally better than 8%.

Zircon Imagery and O Isotope Analysis

Zircon crystals were separated from crushed rocks with standard heavy liquid and magnetic procedures. The divided material was carefully panned and examined under a binocular microscope and representative zircons were picked and mounted in an epoxy resin then polished to expose a near equatorial section. Subsequently, the cathodoluminescence images were obtained using a field-emission scanning electron microprobe (ESCAN MIRA3) at the Tuoyan Analytical Technology Co. Ltd. (Guangzhou, China).

Zircon oxygen isotope analysis was performed using the CAMECA IMS1280 SIMS at the Guangzhou Institute of Geochemistry, Chinese Academy of Sciences following the procedures described by Yang et al. (2018). A focused Cs+ primary ion beam was accelerated at 10 kV, with an intensity of ~2 nA. The spot is ~20 μm in diameter (10 μm primary beam + 10 μm raster). The measured oxygen isotopic data were corrected for instrumental mass fractionation using the Penglai zircon standard ($\delta^{18}O_{\text{Vienna standard mean ocean water}} = 5.31‰$, Li et al., 2010), which was analyzed once every five unknowns. The internal precision of a single analysis was generally better than 0.2‰ (1σ standard error) for the $^{18}O/^{16}O$ ratio. Fifty-three measurements of the Penglai zircon standard during the course of this study yielded a weighted mean of $\delta^{18}O = 5.28 \pm 0.32‰$ (two standard deviations [2SD]), consistent within errors with the reported value of 5.31 ± 0.10‰ (2SD) (Li et al., 2010). Moreover, twelve measurements of the Qinghu zircon standard in this study gave a weighted mean of $\delta^{18}O = 5.49 \pm 0.34‰$ (2SD), which is in agreement with the reported values of 5.39 ± 0.22‰ (2SD) (Li et al., 2013) and 5.46 ± 0.24‰ (2SD) (Yang et al., 2018).

Zircon U-Pb-Hf Isotope Analysis

Zircon U-Pb dating for samples 18MY01, 18MY02, and 18MY03 was performed by a multicollector–inductively coupled plasma–mass spectrometer (MC-ICP-MS) equipped with a Resonetics RESOlution M-50-HR Excimer laser-ablation system at the University of Hong Kong, while other samples were analyzed using an Agilent 7700x laser ablation (LA)-ICP-MS coupled with a RESOlution LR laser-ablation system at the FocuMS Technology Co. Ltd. (Nanjing, China). The analytical procedures and instrument parameters for the two techniques are similar to those in Xia et al. (2011) and Jackson et al. (2004), respectively. Helium was used as a carrier gas, and argon was utilized as the make-up gas and mixed with the carrier gas via a T-connector before entering the ICP. Zircon 91500 was employed as an external standard to calibrate the U-Th-Pb isotopic ratios. Off-line selection and integration of background and analysis signals and time-drift correction and quantitative calibration were calculated using the program ICPMSDataCal 8.0 (Liu et al., 2008). The weighted mean U-Pb ages and concordia diagrams were processed using the Isoplot 3.0 software (Ludwig, 2003). In this study, zircon analyses with concordance <95% are not considered for the mean age calculation.

Analysis of in situ zircon Lu-Hf isotopes was conducted using a Nu Plasma II MC-ICP-MS, equipped with a RESOlution LR laser-ablation system (λ = 193 nm), at the FocuMS Technology Co. Ltd. During analysis, a beam diameter of ~50 μm and a laser repetition rate of 8 Hz were utilized. The obtained $^{176}Hf/^{177}Hf$ ratios were normalized to $^{176}Hf/^{177}Hf = 0.7325$, using an exponential correction for mass bias. Isobaric interference corrections for ^{176}Yb and ^{176}Lu on ^{176}Hf were made by ^{172}Yb and ^{175}Lu, respectively. Ratios used for such corrections were 0.5887 for $^{176}Yb/^{172}Yb$ and 0.02655 for $^{176}Lu/^{175}Lu$ (Vervoort et al., 2004). Standard zircons 91500 and GJ-1 were employed as external standards and analyzed twice before and after every ten analyses. The ^{176}Lu decay constant of 1.867×10^{-11} yr^{-1} (Söderlund et al., 2004) was used to calculate initial $^{176}Hf/^{177}Hf$ ratios, and the chondritic values of $^{176}Hf/^{177}Hf$ (0.282772) and $^{176}Lu/^{177}Hf$ (0.0332) were adopted for the calculation of εHf values (Blichert–Toft and Albarède, 1997). Single-stage Hf model ages (T_{DM1}) were calculated relative to the present-day depleted mantle $^{176}Hf/^{177}Hf$ ratio of 0.283250 and $^{176}Lu/^{177}Hf$ ratio of 0.0384 (Griffin et al., 2000), while two-stage "crustal" model ages (T_{DM2}) were calculated using the mean $^{176}Lu/^{177}Hf$ ratio of 0.015 for the average continental crust (Griffin et al., 2002).

RESULTS

Zircon U-Pb Geochronology

Zircon grains from the Barleik diorite (19BLK01) are prismatic, transparent, and euhedral with lengths of 50–150 μm and length/width ratios of 1:1–3:1 (Fig. 3A). The analyzed zircons (n = 19) exhibit clear oscillatory zonation with high Th/U ratios (0.19–0.49), suggesting an igneous origin. Zircon analyses yield $^{206}Pb/^{238}U$ ages between 496 Ma and 505 Ma (Supplemental Material 1[1]), which form a coherent group and give a weighted mean of 501.6 ± 2.6 Ma (Fig. 3B). Zircon grains from the Barleik granodiorite (19BLK02) are stubby and subhedral, show concentric compositional zoning, and have high Th/U ratios (0.18–0.49), consistent with a magmatic origin. The size of the zircons range from 100 to 200 μm in length with aspect ratios of 1:1–2:1 (Fig. 3A). Twenty-two zircon analyses yield $^{206}Pb/^{238}U$ ages from 494 Ma to 517 Ma, giving a weighted mean of 503.3 ± 3.3 Ma (Fig. 3B).

Figure 3. (A) Cathodoluminescence (CL) images of dated zircon grains showing internal growth zoning and the locations of in situ isotopic analyses. The scale bars in all CL images are 100 μm in length, and the errors for U-Pb ages are quoted at the 2σ level. (B) Zircon U-Pb concordia plots and Th/U (or $^{232}Th/^{238}U$) age diagrams for the felsic and gabbroic (19SLH02) samples from the Barleik-Mayile-Saleinuohai (BMS) ophiolitic mélanges, West Junggar, NW China. The Th/U ratios of samples 19BLK01, 19BLK02, 19MY01, 19SLH02, and 19SLH07 were obtained by laser ablation–inductively coupled plasma–mass spectrometry, since Th and U contents can be directly calculated by element Si signal from standard NIST 610 using this procedure; while the $^{232}Th/^{238}U$ ratios of samples 18MY01, 18MY02, and 18MY03 were obtained by multicollector–inductively coupled plasma–mass spectrometry, as $^{232}Th/^{238}U$ ratios of our samples can be calibrated by $^{232}Th/^{238}U$ of external zircon standard 91500 using this method. Although Th/U is the same as $^{232}Th/^{238}U$, the use of the two phraseologies just indicates two different analytical methods. MSWD—mean square weighted deviation.

[1]Supplemental Material. Table S1: Zircon U-Pb dating results for the felsic and gabbroic plutons from West Junggar, NW China. Table S2: Zircon Hf-O isotope compositions for the felsic and gabbroic plutons from West Junggar, NW China. Table S3: Whole-rock major and trace element compositions for the felsic and gabbroic plutons from West Junggar, NW China. Table S4: Trace element compositions of zircons in the felsic and gabbroic plutons from West Junggar, NW China. Please visit https://doi.org/10.1130/GSAB.S.19134506 to access the supplemental material, and contact editing@geosociety.org with any questions.

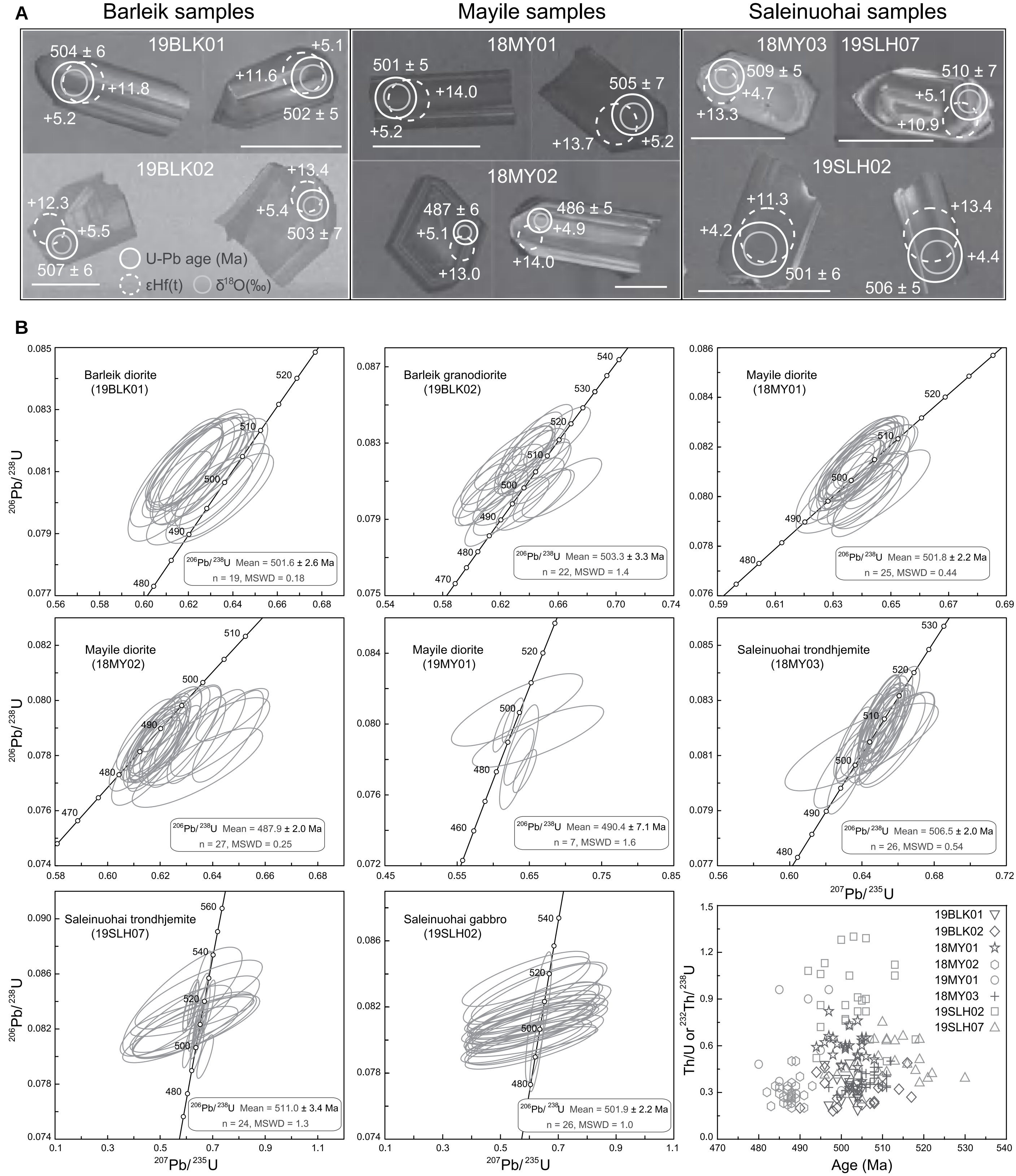

Zircon crystals extracted from three Mayile diorite samples (18MY01, 18MY02, and 19MY01) are subhedral to euhedral, form short or elongate prisms, and range in size from 50 to 250 μm with length-to-width ratios of 1:1–5:1 (Fig. 3A). Most zircons display well-developed oscillatory zoning (Fig. 3A) which, together with the high zircon $^{232}Th/^{238}U$ ratios (0.20–0.82) for samples 18MY01 and

18MY02 and high zircon Th/U ratios (0.31–0.96) for sample 19MY01, indicates a magmatic origin. Twenty-five, twenty-seven, and seven concordant $^{206}Pb/^{238}U$ ages were obtained for samples 18MY01, 18MY02, and 19MY01, respectively, and give weighted mean ages of 501.8 ± 2.2 Ma, 487.9 ± 2.0 Ma, and 490.4 ± 7.1 Ma, respectively (Fig. 3B).

Zircon grains from two Saleinuohai granite samples (18MY03 and 19SLH07) are transparent, and exhibit euhedral forms with crystal lengths varying from 40 to 150 μm and length/width ratios of 1:1–3:1 (Fig. 3A). They show narrow oscillatory zones with high $^{232}Th/^{238}U$ (0.28–0.50) and Th/U (0.31–0.96) ratios for samples 18MY03 and 19SLH07, respectively. Twenty-four and twenty-seven zircons were analyzed for samples 18MY03 and 19SLH07, respectively, yielding weighted mean $^{206}Pb/^{238}U$ ages of 506.5 ± 2.0 Ma and 511.0 ± 3.4 Ma, respectively (Fig. 3B). In contrast, zircons from one Saleinuohai gabbro sample (19SLH02) are stubby and subhedral with lengths of 40–100 μm and aspect ratios of 1:1–2:1 (Fig. 3A). Their broad oscillatory zoning and high Th/U (0.29–1.30) ratios are in line with an igneous origin. The analyses of twenty-six zircons yield $^{206}Pb/^{238}U$ ages from 492 Ma to 518 Ma, with a weighted mean of 501.9 ± 2.2 Ma (Fig. 3B).

Zircon Hf-O Isotopes

All the rocks have high and uniform zircon Hf isotopic compositions, with εHf(t) values mostly between +10 and +14 (Fig. 4A). The two Barleik felsic samples show zircon εHf(t) values of +11.6 to +14.4 with a mean of +12.7 ± 1.4 (the errors for εHf(t) values are quoted at 2SD) and +12.3 to +13.9 with a mean of +13.2 ± 0.98 (Supplemental Material 2). Comparably, the three Mayile felsic samples display zircon εHf(t) values from +10.5 to +12.8 averaging +11.9 ± 1.7, from +11.5 to +14.5 averaging +13.4 ± 1.7, and from +12.7 to +14.2 averaging +13.4 ± 0.88. Zircon εHf(t) values (+10.4 to +13.9 with a mean of +11.7 ± 2.2) for the Saleinuohai gabbro sample fall between those of the two Saleinuohai felsic samples (+10.0 to +13.1 with a mean of +11.5 ± 1.7 and +13.1 to +14.4 with a mean of +13.7 ± 0.88).

The two Barleik felsic samples possess similar zircon O isotopic compositions, with $\delta^{18}O$ values ranging from 5.0 to 5.5‰ with a mean of 5.2 ± 0.28‰ (the errors for $\delta^{18}O$ values are quoted at 2SD) and from 4.9 to 5.7‰ with a mean of 5.4 ± 0.43‰ (Fig. 4B). Likewise, the three Mayile felsic samples have zircon $\delta^{18}O$ values from 5.0 to 5.5‰ (average 5.2 ± 0.31), from 4.8 to 5.4‰ (average 5.1 ± 0.30), and from 4.8 to 5.5‰ (average 5.1 ± 0.39). All of the above O isotope values resemble those (5.3 ± 0.6‰) of zircons in equilibrium with mantle-derived magmas (Valley et al., 1998). For the Saleinuohai rocks, the two felsic samples have mantle-like or slightly lower zircon $\delta^{18}O$ values (4.4–5.3‰ with a mean of 5.0 ± 0.48‰ and 4.5–5.3‰ with a mean of 5.0 ± 0.39‰), whereas the gabbro sample has zircon $\delta^{18}O$ values (4.2–4.7‰ with a mean of 4.5 ± 0.31‰) below the mantle values (Fig. 4B).

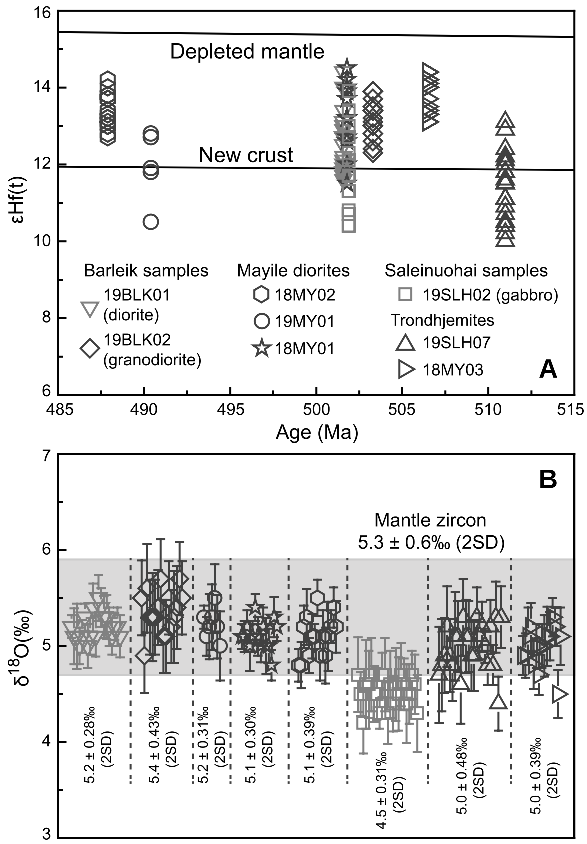

Figure 4. (A) Zircon εHf(t) age diagram for the felsic and gabbroic (19SLH02) samples from the Barleik-Mayile-Saleinuohai (BMS) ophiolitic mélanges, West Junggar, NW China. The depleted mantle (DM) and new crust (NC) lines are from Dhuime et al. (2011), which assumes that the DM and NC reservoirs have linear isotopic growth from εHf(t) = 0 at 4.56 Ga to εHf(t) = 17 at the present for the DM and to εHf(t) = 13.2 at the present for the NC. (B) Zircon $\delta^{18}O$ values for the felsic and gabbroic plutons from the BMS ophiolitic mélanges. Error bars represent two standard deviations (2SD) of each session. The $\delta^{18}O$ range of igneous zircons in equilibrium with mantle magmas is from Valley et al. (1998).

Whole-Rock Geochemistry

Most felsic plutons from the Barleik-Mayile-Saleinuohai ophiolitic mélanges can be compositionally classified as diorite, quartz diorite, granodiorite, tonalite, and trondhjemite (Figs. 5A and 5B). In terms of REE patterns, the felsic rocks from the Barleik mélange can be divided into the high-La/Yb (La/Yb = 27.5–38.4) and low-La/Yb (10.5–11.2) groups (Supplemental Material 3), corresponding to the diorite and granodiorite, respectively. Relative to the high-La/Yb diorites (SiO_2 = 57.9–59.2 wt%, Na_2O = 6.78–7.85 wt%, CaO = 5.45–9.36 wt%), the low-La/Yb granodiorites have higher SiO_2 (62.4–65.6 wt%) and lower Na_2O (4.48–4.99 wt%) and CaO (2.58–4.88 wt%) contents (Figs. 5C–5F). Both the high-La/Yb and low-La/Yb rocks show intermediate Sr (155–428 ppm) and low Y (3.20–7.50 ppm) and Yb (0.25–0.82 ppm) concentrations with high Sr/Y (43.8–102) ratios. In addition, the significantly positive Eu anomalies ($Eu/Eu^* = Eu_N/(Sm_N \times Gd_N)^{1/2} = 2.37–2.89$) of the high-La/Yb diorites are in contrast to the negligible Eu anomalies (Eu/Eu* = 0.93–1.0) of the low-La/Yb granodiorites (Fig. 6A). On the primitive mantle-normalized trace element diagrams (Fig. 6B), the high-La/Yb diorites exhibit depletion in Nb-Zr-Hf-Ti, whereas the low-La/Yb granodiorites display negative Nb-Ti but positive Zr-Hf anomalies.

The gabbros from the Mayile mélange have 49.9–50.3 wt% SiO_2, 2.12–3.10 wt% Na_2O, 0.21–0.25 wt% TiO_2, and 11.0–14.1 wt% CaO (Figs. 5C–5F). Compared to the Mayile gabbros, the Mayile diorites possess higher SiO_2 (53.0–60.9 wt%), Na_2O (2.67–6.56 wt%), and TiO_2 (0.34–0.57 wt%) but lower CaO (mostly <8.0 wt%) contents (Figs. 5C–5F). Both the Mayile gabbros and diorites feature light REE (LREE)-enriched patterns with La/Sm ratios from 2.76 to 5.18 (Fig. 6C). Moreover, the diorite samples have higher REE contents (62.2–151 ppm) than those (20.6–55.6 ppm) of the gabbro samples. As illustrated on Figure 6D, the gabbroic and dioritic rocks display enrichment in LILEs relative to HFSEs, with pronounced Nb, Ta, Zr, and Ti troughs.

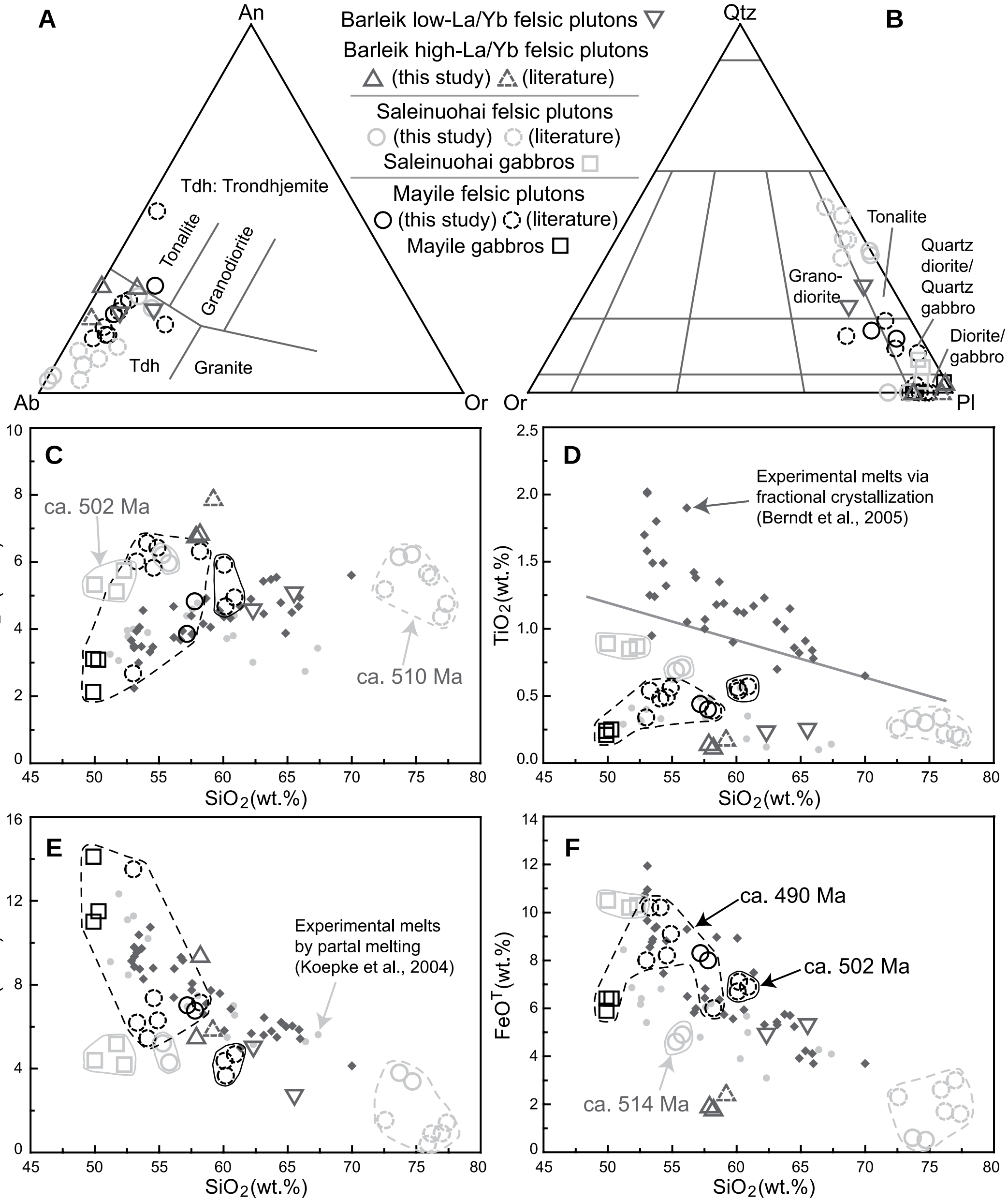

Figure 5. (A) Normative whole-rock (An—anorthite; Ab—albite; Or—orthoclase) ternary diagram (Barker and Arth, 1976) for felsic plutons from the Barleik-Mayile-Saleinuohai ophiolitic mélanges, West Junggar, NW China. (B) Classification of the intrusive rocks using CIPW norms (Le Bas and Streckeisen, 1991). (C) Na_2O, (D) TiO_2, (E) CaO, and (F) FeO^T versus SiO_2 diagrams. Experimental melts formed by fractional crystallization and partial melting of oceanic gabbros are from Berndt et al. (2005) and Koepke et al. (2004), respectively. The dashed line in (D) corresponding to the minimum TiO_2 values from all experiments on mid-ocean ridge basalt differentiation in tholeiitic systems as referred to by Koepke et al. (2007). Tdh—trondhjemite.

In contrast to the Saleinuohai gabbros (SiO_2 = 50.0–52.3 wt%, TiO_2 = 0.85–0.89 wt%, FeO^T = 10.2–10.5 wt%), the Saleinuohai felsic plutons have higher contents of SiO_2 (55.3–77.4 wt%) but lower contents of TiO_2 (0.19–0.71 wt%) and FeO^T (<7.5 wt%) (Figs. 5C–5F). Although both the Saleinuohai gabbroic and felsic samples present LREE-enriched patterns (Fig. 6E), the gabbros show less fractionated LREE (La/Sm = 2.39–3.30) than the felsic rocks (La/Sm = 3.20–7.80). Additionally, the gabbros have weak Eu (Eu/Eu* = 0.89–1.09) and Sr anomalies, distinct from the variable Eu (Eu/Eu* = 0.54–1.11) and Sr anomalies of the felsic rocks (Fig. 6F). On the primitive mantle-normalized multi-element plots (Fig. 6F), the negative Nb, Zr, and Hf anomalies become stronger from the felsic to gabbroic rocks, while the negative Ti anomalies become stronger from the gabbroic to felsic rocks.

DISCUSSION

Diverse Origins of Cambrian Felsic Plutons within West Junggar

Tholeiitic to calc-alkaline dioritic to granitic rocks have been widely documented in oceanic crust and ophiolites, and are generally thought to be formed by differentiation of mid-ocean ridge basalt (MORB) type magmas (Freund et al., 2014; Whattam et al., 2016) or hydrous melting of gabbroic/diabasic oceanic crust (Koepke et al., 2004; Morag et al., 2020). It has been demonstrated that dioritic to granitic melts derived from the latter process feature lower TiO_2 contents than those produced by the former process, because (1) the typical oceanic gabbro is depleted in TiO_2 relative to MORB, resulting in low TiO_2 contents of its melting products (Koepke et al., 2007) and (2) the relatively low magma fugacity (fO_2) in the former process will destabilize iron oxides and consequently lead to high TiO_2 contents in the evolved melts (Berndt et al., 2005). As shown on Figure 5, the studied dioritic to granitic rocks have low TiO_2 contents and plot below the minimum line of TiO_2 content for evolved

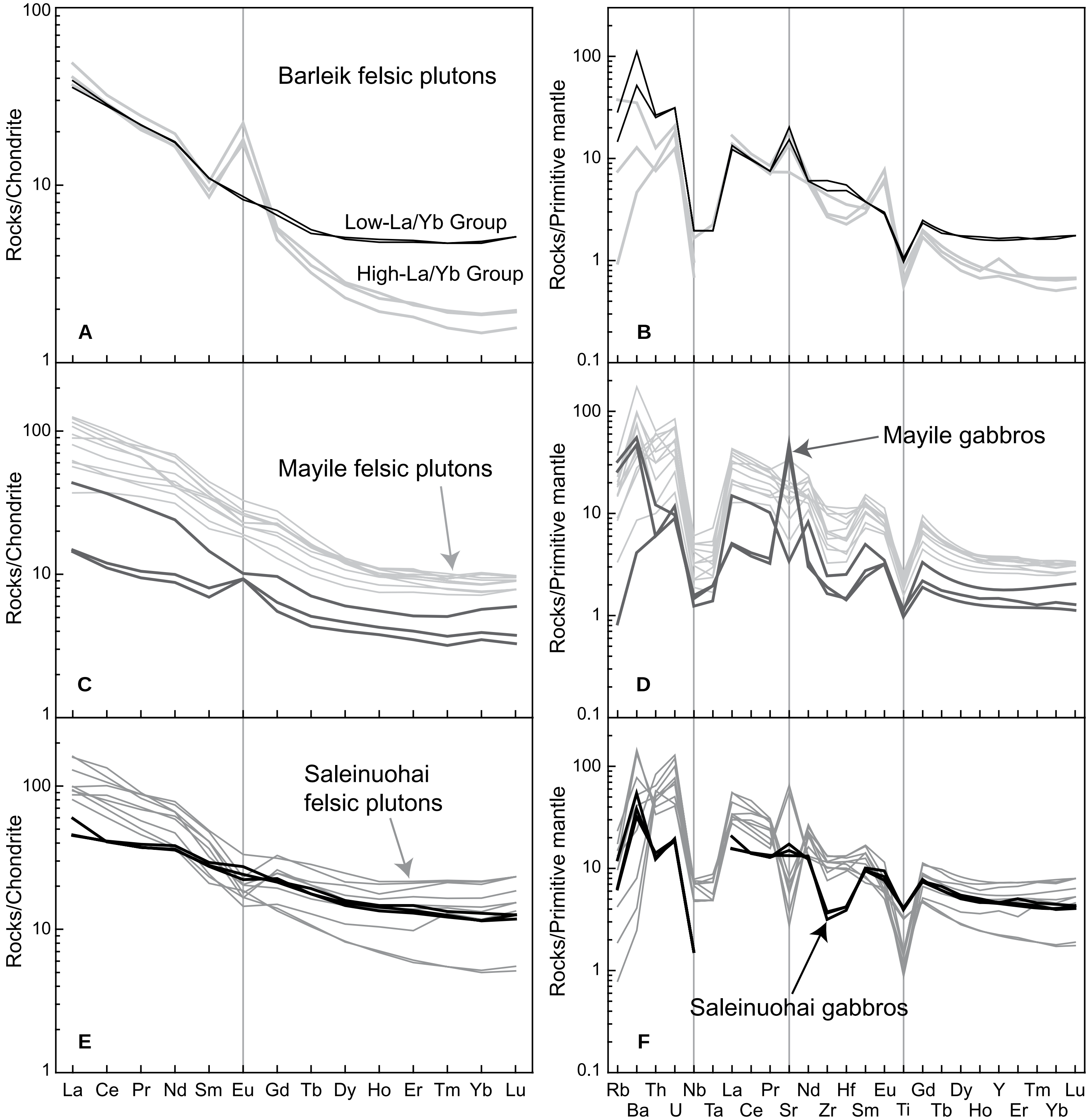

Figure 6. Chondrite-normalized rare earth element and primitive mantle-normalized multi-element patterns for the Cambrian felsic and gabbroic rocks from the Barleik-Mayile-Saleinuohai ophiolitic mélanges, West Junggar, NW China. Normalizing values are from Sun and McDonough (1989).

rocks through fractional crystallization of MORB, indicating that an origin of such rocks by hydrous melting of gabbros is possible. Nevertheless, it is notable that the Barleik-Mayile-Saleinuohai ophiolitic rocks were generated in a subduction setting and arc-derived basalts usually feature lower TiO_2 contents than MORB (Metcalf and Shervais, 2008), thus it is also possible that the studied dioritic to granitic rocks were formed by fractional crystallization of arc basalts that were characterized by low TiO_2. The distinction between differentiation of arc basalts and hydrous melting of gabbroic/diabasic oceanic crust can be effectively discerned by comparing their REE patterns, as

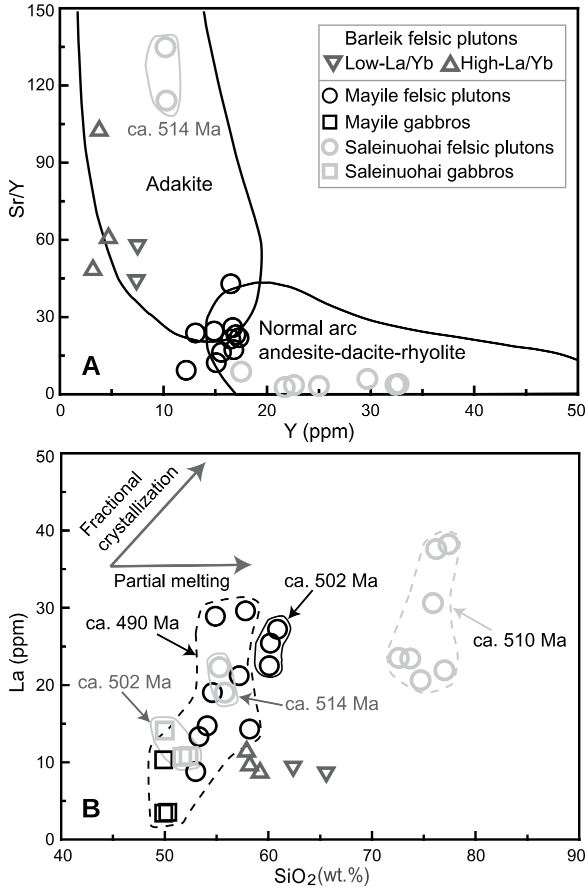

Figure 7. (A) Sr/Y-Y (Defant and Drummond, 1990) and (B) La-SiO_2 diagrams for the Cambrian felsic and gabbroic rocks within the West Junggar, NW China.

melts produced by the former and latter process would show increasing and decreasing/constant La abundances, respectively (Brophy, 2008). This is because D_{La} values for most igneous minerals (e.g., amphibole and pyroxene) increase with increasing liquid SiO_2 contents, which would result in the increase in bulk D_{La} with increasing SiO_2 and consequently lead to increased La concentrations for fractional crystallization and decreased/constant La abundances for partial melting. Accordingly, the combination of TiO_2 contents with REE trends could help ascertain the petrogenesis of dioritic to granitic rocks within ophiolites.

Except for the low and constant TiO_2 contents (Fig. 5D), the La contents of the Barleik dioritic to granodioritic rocks remain constant or even decrease with increasing SiO_2 (Fig. 7), implying that they were likely derived from partial melting of mafic crust. Given that zircons from the Barleik felsic plutons exhibit high εHf(t) (12.7 ± 1.4 to 13.2 ± 0.98) and mantle-like $\delta^{18}O$ (5.2 ± 0.28‰ to 5.4 ± 0.43‰) values, it is inferred that the mafic protolith was juvenile and had not been markedly altered by water-rock interaction (Grimes et al., 2011). In addition, the Barleik felsic rocks are featured by intermediate SiO_2 (57.9–65.6 wt%), high Al_2O_3 (14.1–22.2 wt%) and Sr (mostly >300 ppm), low Y (3.20–7.50 ppm), and high Sr/Y (43.8–102) (Fig. 7A), similar to those of adakites in modern subduction zones (Defant and Drummond, 1990; Martin et al., 2005), suggesting partial melting of mafic photoliths in a subducted slab with garnet ± amphibole as a residual assemblage (Moyen, 2009). In the case of the low-La/Yb granodiorites, their relatively flat middle to heavy REE patterns with low Dy/Yb_N (subscript N presents chondrite normalization) ratios (1.0–1.1) support an amphibolite source (Fig. 6A). By comparison, the high-La/Yb diorites show right-inclined middle to heavy REE patterns with high Dy/Yb_N ratios (1.5–1.6), reflecting the involvement of garnet in the source residue (Davidson et al., 2013). Therefore, it is concluded that during slab melting the source residues of the low-La/Yb granodiorites and high-La/Yb diorites were dominated by amphibole and garnet, respectively.

The Mayile dioritic rocks display positive correlation between SiO_2 and La abundances (Fig. 7B), pointing to fractional crystallization playing a crucial role in their petrogenesis. However, they show significantly low TiO_2 contents, which are different from those differentiated from MORB-type parental magmas (Fig. 5). Instead, the ca. 490 Ma Mayile dioritic rocks exhibit continuous compositional trends with coeval arc-derived gabbros (Fig. 5), supporting an origin via differentiation of arc-related mafic magmas. This explanation is corroborated by prominent removal of plagioclase, as evidenced by the transition from positive Eu-Sr anomalies of gabbros to negligible/negative Eu-Sr anomalies of dioritic rocks (Fig. 6) and the negative correlation of SiO_2 with CaO (Fig. 5). Meanwhile, the TiO_2 and FeO^T contents increase with increasing SiO_2 at $SiO_2 < 55$ wt% and begin to decrease at $SiO_2 > 55$ wt% (Fig. 5), consistent with the initial fractionation of Fe-Ti oxides occurring at $SiO_2 = 55$ wt%. Furthermore, the ca. 490 Ma Mayile dioritic rocks not only present REE patterns similar to but have REE contents higher than those of the synchronous gabbros, providing robust evidence for a derivation from differentiation of arc basalts (Brophy, 2008). For the ca. 502 Ma Mayile dioritic rocks, they feature moderate SiO_2 (60.1–60.9 wt%), low TiO_2 (0.54–0.57 wt %), high MgO (4.17–4.26 wt%) and Mg# (51.2–53.1), intermediate Sr (353–433 ppm) and Sr/Y (21.4–25.9), and high Th/La (0.17–0.22), making them akin to sanukitoids in the Setouchi volcanic belt, SW Japan (Shimoda et al., 1998). Accordingly, an analogous mechanism is proposed that silicic melts from partial melting of subducted sediments metasomatized the fore-arc mantle wedge and subsequent melting produced the ca. 502 Ma Mayile dioritic rocks. Resembling the Barleik felsic rocks, all of the Mayile ones possess high zircon εHf(t) (11.9 ± 1.7–13.4 ± 0.88) and mantle-like zircon $\delta^{18}O$ (5.1 ± 0.30‰ to 5.2 ± 0.31‰) values, which may reflect that the Mayile dioritic rocks formed either by differentiation of arc magmas or by partial melting of a metasomatized mantle wedge that were in oxygen isotopically equilibrium with the mantle (Grimes et al., 2011).

All the Saleinuohai felsic rocks are characterized by low TiO_2 contents, below the limit for experimental MORB fractionation (Fig. 5). This can be regarded as a diagnostic indicator of felsic rocks generated by hydrous melting of mafic crust (France et al., 2010; Koepke et al., 2007). As shown on Figure 7A, the ca. 514 Ma Saleinuohai dioritic rocks ($SiO_2 = 55.3$–55.8 wt%) have high Sr (1175–1375 ppm), low Y (10.2–10.3 ppm), and high Sr/Y (114–134), typical features of slab-derived adakites. Additionally, their Dy/Yb_N ratios (1.60–1.63) are obviously greater than one, demonstrating the partial melting of basaltic crust in the slab under an eclogite-facies condition (Davidson et al., 2013). For the ca. 510 Ma Saleinuohai trondhjemitic rocks, they have high SiO_2 (72.6–77.4 wt%), low MgO (0.09–1.49 wt%) and Sr (57.9–176 ppm), high Y (17.5–32.7 ppm), and low Sr/Y (2.7–8.8), resembling normal arc rhyolites and thus implying an origination from partial melting of arc mafic crust. Besides, the ca. 510 Ma Saleinuohai trondhjemitic rocks show zircon $\delta^{18}O$ values (4.4–5.3‰ and 4.5–5.3‰) similar to or mildly lower than mantle values (5.3 ± 0.6‰), and the handful of low-$\delta^{18}O$ values require a minor contribution of arc mafic crust that had interacted with seawater/fluids at high temperature (Grimes et al., 2013; Morag et al., 2020).

As a whole, the Cambrian felsic plutons within West Junggar involve diverse origins, including slab melting for the 503–501 Ma Barleik dioritic to granodioritic rocks and the ca. 514 Ma Saleinuohai dioritic rocks, fractional crystallization of arc basalts for the ca. 490 Ma Mayile dioritic rocks, partial melting of arc mafic crust for the ca. 510 Ma Saleinuohai trondhjemitic rocks, and a metasomatized mantle wedge for the ca. 502 Ma Mayile dioritic rocks.

Petrogenesis of the Saleinuohai Gabbros

The ca. 502 Ma Saleinuohai gabbros, with SiO_2 contents from 50.0 to 52.3 wt%, are characterized by high Na_2O (5.11–5.74 wt%) and $Fe_2O_3^T$ (11.3–11.7 wt%), low K_2O (0.43–0.69 wt%), MgO (3.57–4.39 wt%), and Ni (<3 ppm), sharing affinities with low-K tholeiites (Ishizuka et al., 2006; Kimura and Yoshida, 2006). Given the incompatibility of Nb relative to Zr, the partial melting of mantle could result in a residuum with high Zr/Nb ratios. For the ca. 502 Ma Saleinuohai gabbros, their Zr/Nb ratios (32.3–38.2) are remarkably higher (Zr/Nb = 15.7, Sun and McDonough, 1989) than that of the primitive mantle which, coupled with their depleted zircon εHf(t) values (+11.7 ± 2.2), demonstrates a depleted mantle source. Moreover, their positive anomalies of U and Ba, and negative anomalies of Nb and Ti as well as relatively variable Ba/La (20.9–27.1) but constant Th/Yb (0.53–0.56) suggest that the depleted mantle source had been metasomatized by slab fluids (Woodhead et al., 2001; Pearce, 2008). This inference is confirmed by the significant depletion in Hf relative to Sm ($(Hf/Sm)_N = 0.38–0.44$), since Sm is much more soluble than Hf in aqueous fluids (La Flèche et al., 1998). Noteworthily, the gabbro sample exhibits zircon $\delta^{18}O$ values from 4.2‰ to 4.7‰ with a mean of 4.5 ± 0.31‰, which are below those of zircons in equilibrium with mantle (5.3 ± 0.6‰, Valley et al., 1998) and thus reflect that the depleted mantle source had been hydrated by hydrothermal fluids with seawater-like oxygen isotopes at high temperature (Grimes et al., 2013; Yu et al., 2020).

Early Subduction Records in the Western Paleo-Asian Ocean

The Central Asian Orogenic Belt comprises three collage systems, including the Mongolia system in the north, the Tarim-North China system in the south, and the Kazakhstan system in the west (Wilhem et al., 2012; Xiao et al., 2015). By integrating data of paleolatitudes and distribution of biocenoses, it is indicated that the three collage systems were separated far from each other at least before Silurian (Xiao et al., 2015). The Kazakhstan collage system, formed by the welding of multiple orogenic components (Fig. 8A) as the result of consumption of the western Paleo-Asian Ocean, is characterized by the occurrence of tight oroclines (Levashova et al., 2003; Li et al., 2018). Available paleomagnetic data have revealed that the Kazakhstan landmass (i.e., the Ishim-Middle Tianshan/Stepnyak-North Tianshan (IMT/SNT) microcontinent) and the Mariana-type Boshchekul-Chingiz (BC) island arc were located at the same (~10°S) latitude in the early to middle Paleozoic period, constituting a ~E-W–trending composite belt prior to oroclinal bending (Fig. 8B, Alexyutin et al., 2005; Bazhenov et al., 2012). In the late Paleozoic, this composite belt attained its U-shaped structure via oroclinal bending with the ~180° clockwise rotation of the northern limb relative to the southern limb (Van der Voo et al., 2006; Levashova et al., 2007). As the oldest subduction records in the Kazakhstan collage system (Fig. 8A), the Cambrian arc rocks and accretionary complexes developed on this quasi-linear composite belt could provide pivotal constraints on the initial subduction of the western Paleo-Asian Ocean.

It has been reported that both the Kazakhstan landmass and the BC oceanic arc contain Cambrian SSZ-type ophiolitic mélanges (e.g., 530 Ma Kopu-relisay ophiolites, Kröner et al., 2012), arc magmas (e.g., 514 Ma Makbal granodiorite, Konopelko et al., 2012), and subduction-related metamorphic rocks (e.g., 509 Ma Makbal eclogite, Konopelko et al., 2012), strongly implying the presence of an active margin beneath the IMT/SNT-BC range during Early to Middle Cambrian (Fig. 8A). The southern West Junggar, located to the southeast (present coordinates) of the BC island arc, consists of contemporaneous SSZ-type ophiolites (e.g., Early-Middle Cambrian Barleik-Mayile-Saleinuohai ophiolite, Ren et al., 2014 and this study) and slab-derived adakitic silicic rocks (e.g., 514 Ma Saleinuohai adakite, this study), which may suggest that the southern West Junggar might be a part of the BC arc (Fig. 8B). Therefore, it is possible that a long (>1000 km) Mariana-type arc subduction system (i.e., BC–southern West Junggar) existed in the western Paleo-Asian Ocean during the Early-Middle Cambrian. This is consistent with the modeling results, which suggest Mariana-type subduction initiation could be at the scale of >1000 km (Maunder et al., 2020). If this is the case, the early subduction records in the current study and previous studies may mark the initiation of subduction of the western Paleo-Asian Ocean in the Early Cambrian (Fig. 8C).

Subduction Initiation of the Western Paleo-Asian Ocean in a Global Context

Although the driving mechanisms of subduction initiation in accretionary orogens have not been fully illuminated, it is gradually recognized that subduction initiation in accretionary orogens coincides with global tectonic adjustments (e.g., supercontinent assembly or break-up, Cawood and Buchan, 2007; Ulvrova et al., 2019a, 2019b; Yao et al., 2021). The global plate reorganizations associated with supercontinent assembly or break-up commonly involve plate acceleration and reorientation, which may result in nucleation of new subduction zones over a long distance. For example, Cawood and Buchan (2007) pointed out that collision of continental blocks during supercontinent assembly would reduce the convergence velocity between the blocks and change the plate motions between the supercontinent and its peripheral oceanic lithosphere and consequently lead to subduction initiation and accretionary orogenesis. It has been suggested that changes in Pacific plate motions have induced the Eocene subduction initiation at the Paleo-Asian Ocean, Tonga-Kermadec, and New Caledonia arcs (Bache et al., 2012). Besides, Yao et al. (2021) proposed that the final Gondwana assembly had caused the northward initial subduction of the Proto-Tethys oceanic lithosphere. The subduction initiation corresponding to supercontinent assembly has been substantiated by numerical modeling results that indicate Mariana-type oceanic subduction initiation is more prevalent during times of supercontinent assembly due to the decreased lengths of continental margins (Ulvrova et al., 2019a). Also, modeling studies have indicated that the synrift phase with an abrupt increase of extension rates during supercontinent break-up could enhance convergence rates and episodic subduction initiation (Ulvrova et al., 2019b). For example, Maffione and van Hinsbergen (2018) proposed that the far-field forces related to the opening of the Alpine Tethys Ocean might have triggered the Middle Jurassic subduction initiation in the Balkan region. Consequently, plate reorganizations correlated with supercontinent

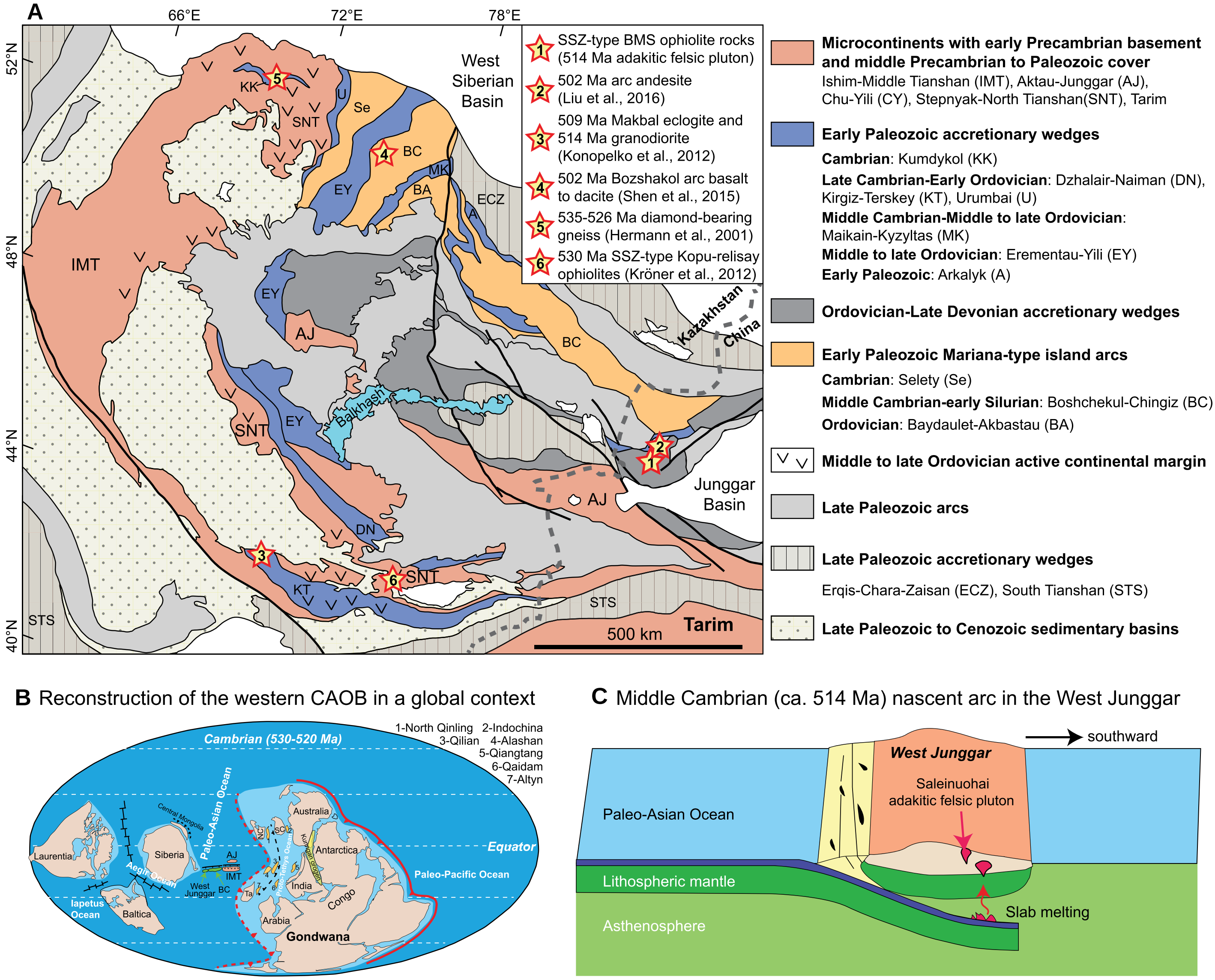

Figure 8. (A) Paleozoic tectonic terranes in the west Central Asian Orogenic Belt (CAOB) showing records of Cambrian arc rocks, ophiolitic rocks, and metamorphic rocks as red stars (after Xiao et al., 2015; Zhang et al., 2018a). (B) Schematic reconstruction for the western CAOB in a global setting during the Middle Cambrian (after Bazhenov et al., 2012; Merdith et al., 2021; Wu et al., 2020; Yao et al., 2021; Zhao et al., 2018). AJ—Aktau-Junggar block; BC—Boshchekul-Chingiz arc; IMT—Ishim-Middle Tianshan block; NC—North China; SC—South China; Ta—Tarim. (C) Section view of the nature and evolution of the West Junggar, NW China, during the Middle Cambrian. SSZ—suprasubduction zone.

assembly or break-up are capable of inducing initial subduction in accretionary orogens.

In the Paleo-Asian Ocean oceanic arc system, 6–8 m.y. is required for production of island-arc tholeiitic to calc-alkaline magmatism since subduction initiation (Ishizuka et al., 2011; Reagan et al., 2013). Comparatively, the initial subduction in the southern West Junggar probably occurred in the Early Cambrian (>520 Ma), as the earliest island-arc tholeiitic adakitic plutons took place at ca. 514–511 Ma (Ren et al., 2014 and this study). In combination with other early subduction records in the western Paleo-Asian Ocean (Fig. 8, e.g., Kröner et al., 2012), it is suggested that initial stages of subduction in the main branch of the western Paleo-Asian Ocean took place between 530 and 520 Ma. It is notable that the Early Cambrian Mariana-type initial subduction in the western Paleo-Asian Ocean was almost synchronous with the terminal stages of Gondwana assembly (ca. 550–520 Ma, Collins and Pisarevsky, 2005; Cawood and Buchan, 2007) and break-up of Laurasia (ca. 570–530 Ma) (Cawood et al., 2001). The ultimate generation of Greater Gondwana was recorded by the 550–520 Ma granulite-facies metamorphism and contractional deformation on both the west and east India that mark the collision between India and the Congo block and between India and the Australia-East Antarctica craton (Meert, 2003; Collins and Pisarevsky, 2005). At the same time, the breakup of Laurasia led to the opening of the Aegir Ocean between Siberia and Baltica and the Iapetus Ocean between Baltica and Laurentia (Cawood et al., 2001). The final change from rifting to passive margin sedimentation around Laurentia, Baltica, and Siberia did not take place until the Early Cambrian at ca. 530 Ma (Cawood et al., 2001). Taken together, temporal relations imply that the initial subduction of the western Paleo-Asian Ocean was probably related to global plate re-adjustments (e.g., plate acceleration and reorientation) that were caused by the eventual assembly of Gondwana and breakup of Laurasia (Fig. 8).

CONCLUSIONS

The Cambrian felsic plutons from the Barleik-Mayile-Saleinuohai ophiolites, West Junggar, show wide SiO_2 contents (53.0–77.4 wt%) and can be classified as diorite, granodiorite, tonalite, and trondhjemite. Based on their low TiO_2 contents, unique trace element trends (e.g., increasing or constant La abundances with increasing SiO_2), high zircon εHf(t) (+10.5 to +14.5), and mantle-like zircon $\delta^{18}O$ (5.0 ± 0.48‰ to 5.4 ± 0.43‰) ratios, it is implied that they have diverse origins, including slab melting for the 503–501 Ma Barleik dioritic to granodioritic rocks and the ca. 514 Ma Saleinuohai dioritic rocks, differentiation of arc basalts for the ca. 490 Ma Mayile dioritic rocks, and partial melting of arc mafic crust for the ca. 510 Ma Saleinuohai trondhjemitic rocks and of metasomatized mantle wedge for the ca. 502 Ma Mayile dioritic rocks. Gabbros from the Saleinuohai area display zircon $\delta^{18}O$ values from 4.2‰ to 4.7‰ lower than those of zircons in equilibrium with mantle, suggesting hydration of their mantle source by hydrothermal fluids at high temperature. In combination with regional geological data (e.g., Early Cambrian SSZ-type ophiolites and felsic intrusions), we propose that the West Junggar arc might have been a part of the BC arc during the Early Cambrian, constituting a ~E-W–trending subduction zone. The earliest island-arc tholeiitic felsic plutons from the Barleik-Mayile-Saleinuohai ophiolitic mélanges formed at ca. 514 Ma which, together with other early subduction records in the western Paleo-Asian Ocean (Fig. 8), suggest subduction of the western Paleo-Asian Ocean probably initiated in the Early Cambrian. The simultaneity between the initial subduction of the western Paleo-Asian Ocean and the terminal stages of Gondwana assembly and Laurasia breakup indicates a causal link between them, probably related to global plate adjustments.

ACKNOWLEDGMENTS

This manuscript benefited from discussion with Xiangsong Wang and Jien Zhang. We thank Jianfeng Gao and Jean Wong for their help with the zircon U-Pb-Hf isotope analyses. We thank Editor Brad S. Singer and Associate Editor Haibo Zou for their kind editorial help and constructive comments. We are grateful to Chong Ma and one anonymous reviewer, whose insightful and constructive reviews greatly improve this manuscript. This work is financially supported by the Key Scientific Issues of Transformative Technology (2019YFA0708601), National Key Research and Development Program of China (2017YFC0601205), the Fund from the Key Laboratory of Deep-Earth Dynamics of Ministry of Natural Resources (J1901-5), the National Science Foundation of China (41873060, 41830216, 41973021), Key Special Project for Introduced Talents Team of Southern Marine Science and Engineering Guangdong Laboratory (Guangzhou, China) (GML2019ZD0104), Guangdong National Science Foundation research team project (2017A030312002), K.C. Wong Education Foundation (GJTD-2018-13), the China Geological Survey (DD20190001, DD20190004) and the Hong Kong RGC research projects (17303415, 17302317). This is a contribution to International Geoscience Programme 662.

REFERENCES CITED

Alexyutin, M.V., Bachtadse, V., Alexeiev, D.V., and Nikitina, O.I., 2005, Palaeomagnetism of Ordovician and Silurian rocks from the Chu-Yili and Kendyktas mountains, south Kazakhstan: Geophysical Journal International, v. 162, p. 321–331, https://doi.org/10.1111/j.1365-246X.2005.02533.x.

Arculus, R.J., Ishizuka, O., Bogus, K.A., Gurnis, M., Hickey-Vargas, R., Aljahdali, M.H., Bandini-Maeder, A.N., Barth, A.P., Brandl, P.A., Drab, L., do Monte Guerra, R., Hamada, M., Jiang, F.Q., Kanayama, K., Kender, S., Kusano, Y., Li, H., Loudin, L.C., Maffione, M., Marsaglia, K.M., McCarthy, A., Meffre, S., Morris, A., Neuhaus, M., Savov, I.P., Sena, C., Tepley, F.J., III, van der Land, C., Yogodzhinski, G.M., and Zhang, Z.H., 2015, A record of spontaneous subduction initiation in the Izu-Bonin-Mariana arc: Nature Geoscience, v. 8, p. 728–733, https://doi.org/10.1038/ngeo2515.

Bache, F., Sutherland, R., Stagpoole, V., Herzer, R., Collot, J., and Rouillard, P., 2012, Stratigraphy of the southern Norfolk Ridge and the Reinga Basin: A record of initiation of Tonga-Kermadec-Northland subduction in the Southwest Pacific: Earth and Planetary Science Letters, v. 321–322, p. 41–53, https://doi.org/10.1016/j.epsl.2011.12.041.

Bai, W.J., Robinson, P., Yang, J.S., Zhou, M.F., and Hu, X.F., 1995, Tectonic evolution of different dating ophiolites in the Western Junggar, Xinjiang: Yanshi Xuebao, v. 11, p. 62–72.

Barker, F., and Arth, J.G., 1976, Generation of trondhjemitic-tonalitic liquids and Archean bimodal trondhjemite-basalt suites: Geology, v. 4, p. 596–600, https://doi.org/10.1130/0091-7613(1976)4<596:GOTLAA>2.0.CO;2.

Bazhenov, M.L., Levashova, N.M., Degtyarev, K.E., Van der Voo, R., Abrajevitch, A.V., and McCausland, P.J.A., 2012, Unraveling the early-middle Paleozoic paleogeography of Kazakhstan on the basis of Ordovician and Devonian paleomagnetic results: Gondwana Research, v. 22, p. 974–991, https://doi.org/10.1016/j.gr.2012.02.023.

Berndt, J., Koepke, J., and Holtz, F., 2005, An experimental investigation of the influence of water and oxygen fugacity on differentiation of MORB at 200 MPa: Journal of Petrology, v. 46, p. 135–167, https://doi.org/10.1093/petrology/egh066.

Blichert-Toft, J., and Albarède, F., 1997, The Lu-Hf isotope geochemistry of chondrites and the evolution of the mantle–crust system: Earth and Planetary Science Letters, v. 148, p. 243–258, https://doi.org/10.1016/S0012-821X(97)00040-X.

Brophy, J.G., 2008, A study of rare earth element (REE)–SiO_2 variations in felsic liquids generated by basalt fractionation and amphibolite melting: A potential test for discriminating between the two different processes: Contributions to Mineralogy and Petrology, v. 156, p. 337–357, https://doi.org/10.1007/s00410-008-0289-x.

Buckman, S., and Aitchison, J.C., 2001, Middle Ordovician (Llandeilan) radiolarians from West Junggar, Xinjiang, China: Micropaleontology, v. 47, p. 359–367, https://doi.org/10.2113/47.4.359.

Cawood, P.A., and Buchan, C., 2007, Linking accretionary orogenesis with supercontinent assembly: Earth-Science Reviews, v. 82, p. 217–256, https://doi.org/10.1016/j.earscirev.2007.03.003.

Cawood, P.A., McCausland, P.J.A., and Dunning, G.R., 2001, Opening Iapetus: Constraints from the Laurentian margin in Newfoundland: Geological Society of America Bulletin, v. 113, p. 443–453, https://doi.org/10.1130/0016-7606(2001)113<0443:OICFTL>2.0.CO;2.

Cawood, P.A., Strachan, R.A., Pisarevsky, S.A., Gladkochub, D.P., and Murphy, J.B., 2016, Linking collisional and accretionary orogens during Rodinia assembly and breakup: Implications for models of supercontinent cycles: Earth and Planetary Science Letters, v. 449, p. 118–126, https://doi.org/10.1016/j.epsl.2016.05.049.

Chen, B., and Arakawa, Y., 2005, Elemental and Nd-Sr isotopic geochemistry of granitoids from the West Junggar foldbelt (NW China), with implications for Phanerozoic continental growth: Geochimica et Cosmochimica Acta, v. 69, p. 1307–1320, https://doi.org/10.1016/j.gca.2004.09.019.

Chen, J.F., Han, B.F., Zhang, L., Xu, Z., Liu, J.L., Qu, W.J., Li, C., Yang, J.H., and Yang, Y.H., 2015, Middle Paleozoic initial amalgamation and crustal growth in the West Junggar (NW China): Constraints from geochronology, geochemistry and Sr-Nd-Hf-Os isotopes of calc-alkaline and alkaline intrusions in the Xiemisitai-Saier Mountains: Journal of Asian Earth Sciences, v. 113, p. 90–109, https://doi.org/10.1016/j.jseaes.2014.11.028.

Choulet, F., Faure, M., Cluzel, D., Chen, Y., Lin, W., Wang, B., and Jahn, B.M., 2012, Architecture and evolution of accretionary orogens in the Altaids collage: The early Paleozoic West Junggar (NW China): American Journal of Science, v. 312, p. 1098–1145, https://doi.org/10.2475/10.2012.02.

Collins, A.S., and Pisarevsky, S.A., 2005, Amalgamating eastern Gondwana: The evolution of the Circum-Indian Orogens: Earth-Science Reviews, v. 71, p. 229–270, https://doi.org/10.1016/j.earscirev.2005.02.004.

Davidson, J., Turner, S., and Plank, T., 2013, Dy/Dy*: Variations arising from mantle sources and petrogenetic processes: Journal of Petrology, v. 54, p. 525–537, https://doi.org/10.1093/petrology/egs076.

Defant, M.J., and Drummond, M.S., 1990, Derivation of some modern arc magmas by melting of young subducted lithosphere: Nature, v. 347, p. 662–665, https://doi.org/10.1038/347662a0.

Dhuime, B., Hawkesworth, C., and Cawood, P., 2011, When continents formed: Science, v. 331, p. 154–155, https://doi.org/10.1126/science.1201245.

Ernst, R.E., Hamilton, M.A., Soderlund, U., Hanes, J.A., Gladkochub, D.P., Okrugin, A.V., Kolotilina, T., Mekhonoshin, A.S., Bleeker, W., LeCheminant, A.N., Buchan, K.L., Chamberlain, K.R., and Didenko, A.N., 2016, Long-lived connection between southern Siberia and northern Laurentia in the Proterozoic: Nature Geoscience, v. 9, p. 464–469, https://doi.org/10.1038/ngeo2700.

France, L., Koepke, J., Ildefonse, B., Cichy, S., and Deschamps, F., 2010, Hydrous partial melting in the sheeted dike complex at fast spreading ridges: Experimental and natural observations: Contributions to Mineralogy and Petrology, v. 160, p. 683–704, https://doi.org/10.1007/s00410-010-0502-6.

Freund, S., Haase, K.M., Keith, M., Beier, C., and Garbe-Schönberg, D., 2014, Constraints on the formation of geochemically variable plagiogranite intrusions in the Troodos Ophiolite, Cyprus: Contributions to Mineralogy and Petrology, v. 167, p. 1–22, https://doi.org/10.1007/s00410-014-0978-6.

Geng, H.Y., Sun, M., Yuan, C., Xiao, W.J., Xian, W.S., Zhao, G.C., Zhang, L.F., Wong, K., and Wu, F.Y., 2009, Geochemical, Sr-Nd and zircon U-Pb-Hf isotopic studies of Late Carboniferous magmatism in the West Junggar, Xinjiang: Implications for ridge subduction?: Chemical Geology, v. 266, p. 364–389, https://doi.org/10.1016/j.chemgeo.2009.07.001.

Griffin, W.L., Pearson, N.J., Belousova, E., Jackson, S.E., Achterbergh, E., O'Reilly, S.Y., and Shee, S.R., 2000, The Hf isotope composition of cratonic mantle: LAM-MC-ICPMS analysis of zircon megacrysts in kimberlites: Geochimica et Cosmochimica Acta,

v. 64, p. 133–147, https://doi.org/10.1016/S0016-7037(99)00343-9.

Griffin, W.L., Wang, X., Jackson, S.E., Pearson, N.J., O'Reilly, S.Y., Xu, X.S., and Zhou, X.M., 2002, Zircon chemistry and magma mixing, SE China: In-situ analysis of Hf isotopes, Tonglu and Pingtan igneous complexes: Lithos, v. 61, p. 237–269, https://doi.org/10.1016/S0024-4937(02)00082-8.

Grimes, C.B., Ushikubo, T., John, B.E., and Valley, J.W., 2011, Uniformly mantle-like $\delta^{18}O$ in zircons from oceanic plagiogranites and gabbros: Contributions to Mineralogy and Petrology, v. 161, p. 13–33, https://doi.org/10.1007/s00410-010-0519-x.

Grimes, C.B., Ushikubo, T., Kozdon, R., and Valley, J.W., 2013, Perspectives on the origin of plagiogranite in ophiolites from oxygen isotopes in zircon: Lithos, v. 179, p. 48–66, https://doi.org/10.1016/j.lithos.2013.07.026.

Hermann, J., Rubatto, D., Korsakov, A., and Shatsky, V.S., 2001, Multiple zircon growth during fast exhumation of diamondiferous, deeply subducted continental crust (Kokchetav Massif, Kazakhstan): Contributions to Mineralogy and Petrology, v. 141, p. 66–82, https://doi.org/10.1007/s004100000218.

Ishizuka, O., Kimura, J.I., Li, Y.B., Stern, R.J., Reagan, M.K., Taylor, R.N., Ohara, Y., Bloomer, S.H., Ishii, T., Hargrove, U.S., III, and Haraguchi, S., 2006, Early stages in the evolution of Izu-Bonin arc volcanism: New age, chemical, and isotopic constraints: Earth and Planetary Science Letters, v. 250, p. 385–401, https://doi.org/10.1016/j.epsl.2006.08.007.

Ishizuka, O., Tani, K., Reagan, M.K., Kanayama, K., Unimo, S., Harigane, Y., Sakamoto, I., Miyajima, Y., Yuasa, M., and Dunkley, D.J., 2011, The timescales of subduction initiation and subsequent evolution of an oceanic island arc: Earth and Planetary Science Letters, v. 306, p. 229–240, https://doi.org/10.1016/j.epsl.2011.04.006.

Ishizuka, O., Tani, K., and Reagan, M.K., 2014, Izu-Bonin-Mariana forearc crust as a modern ophiolite analogue: Elements, v. 10, p. 115–120, https://doi.org/10.2113/gselements.10.2.115.

Jackson, S.E., Pearson, N.J., Griffin, W.L., and Belousova, E.A., 2004, The application of laser ablation-inductively coupled plasma-mass spectrometry to in situ U-Pb zircon geochronology: Chemical Geology, v. 211, p. 47–69, https://doi.org/10.1016/j.chemgeo.2004.06.017.

Jahn, B.M., Wu, F.Y., and Chen, B., 2000, Massive granitoid generation in Central Asia: Nd isotope evidence and implication for continental growth in the Phanerozoic: Episodes, v. 23, p. 82–92, https://doi.org/10.18814/epiiugs/2000/v23i2/001.

Kelemen, P.B., and Manning, C.E., 2015, Reevaluating carbon fluxes in subduction zones, what goes down, mostly comes up: Proceedings of the National Academy of Sciences of the United States of America, v. 112, p. E3997–E4006, https://doi.org/10.1073/pnas.1507889112.

Kessel, R., Schmidt, M.W., Ulmer, P., and Pettke, T., 2005, Trace element signature of subduction-zone fluids, melts and supercritical liquids at 120–180 km depth: Nature, v. 437, p. 724–727, https://doi.org/10.1038/nature03971.

Kimura, J.I., and Yoshida, T., 2006, Contributions of slab fluid, mantle wedge and crust to the origin of Quaternary lavas in the NE Japan arc: Journal of Petrology, v. 47, p. 2185–2232, https://doi.org/10.1093/petrology/egl041.

Koepke, J., Feig, S.T., Snow, J., and Freise, M., 2004, Petrogenesis of oceanic plagiogranites by partial melting of gabbros: An experimental study: Contributions to Mineralogy and Petrology, v. 146, p. 414–432, https://doi.org/10.1007/s00410-003-0511-9.

Koepke, J., Berndt, J., Feig, S.T., and Holtz, F., 2007, The formation of SiO_2-rich melts within the deep oceanic crust by hydrous partial melting of gabbros: Contributions to Mineralogy and Petrology, v. 153, p. 67–84, https://doi.org/10.1007/s00410-006-0135-y.

Konopelko, D., Kullerud, K., Apayarov, F., Sakiev, K., Baruleva, O., Ravna, E., and Lepekhina, E., 2012, SHRIMP zircon chronology of HP-UHP rocks of the Makbal metamorphic complex in the Northern Tien Shan, Kyrgyzstan: Gondwana Research, v. 22, p. 300–309, https://doi.org/10.1016/j.gr.2011.09.002.

Kröner, A., Alexeiev, D.V., Hegner, E., Rojas-Agramonte, Y., Corsini, M., Chao, Y., Wong, J., Windley, B.F., Liu, D., and Tretyakov, A.A., 2012, Zircon and muscovite ages, geochemistry, and Nd-Hf isotopes for the Aktyuz metamorphic terrane: Evidence for an Early Ordovician collisional belt in the northern Tianshan of Kyrgyzstan: Gondwana Research, v. 21, p. 901–927, https://doi.org/10.1016/j.gr.2011.05.010.

Kuzmichev, A.B., Kröner, A., Hegner, E., Liu, D.Y., and Wan, Y.S., 2005, The Shishkhid ophiolite, northern Mongolia: A key to the reconstruction of a Neoproterozoic island-arc system in central Asia: Precambrian Research, v. 138, p. 125–150, https://doi.org/10.1016/j.precamres.2005.04.002.

La Flèche, M.R., Camire, G., and Jenner, G.A., 1998, Geochemistry of post-Acadian, Carboniferous continental intraplate basalts from the Maritimes Basin, Magdalen islands, Quebec, Canada: Chemical Geology, v. 148, p. 115–136, https://doi.org/10.1016/S0009-2541(98)00002-3.

Le Bas, M.J., and Streckeisen, A.L., 1991, The IUGS systematics of igneous rocks: Journal of the Geological Society, v. 148, p. 825–833, https://doi.org/10.1144/gsjgs.148.5.0825.

Levashova, N.M., Degtyarev, K.E., Bazhenov, M.L., Collins, A.Q., and Van der Voo, R., 2003, Middle Paleozoic paleomagnetism of east Kazakhstan: post-Middle Devonian rotations in a large-scale orocline in the central Ural-Mongol belt: Tectonophysics, v. 377, p. 249–268, https://doi.org/10.1016/j.tecto.2003.09.013.

Levashova, N.M., Mikolaichuk, A.V., McCausland, P.J.A., Bazhenov, M.L., and Van der Voo, R., 2007, Devonian paleomagnetism of the North Tien Shan: Implications for the middle-Late Paleozoic paleogeography of Eurasia: Earth and Planetary Science Letters, v. 257, p. 104–120, https://doi.org/10.1016/j.epsl.2007.02.025.

Li, P.F., Sun, M., Rosenbaum, G., Yuan, C., Safonova, I., Cai, K.D., Jiang, Y.D., and Zhang, Y.Y., 2018, Geometry, kinematics and tectonic models of the Kazakhstan Orocline, Central Asian Orogenic Belt: Journal of Asian Earth Sciences, v. 153, p. 42–56, https://doi.org/10.1016/j.jseaes.2017.07.029.

Li, X.H., Long, W.G., Li, Q.L., Liu, Y., Zheng, Y.F., Yang, Y.H., Chamberlain, K.R., Wan, D.F., Guo, C.F., and Wang, X.C., 2010, Penglai zircon megacrysts: A potential new working reference material for microbeam determination of Hf-O isotopes and U-Pb age: Geostandards and Geoanalytical Research, v. 34, p. 117–134, https://doi.org/10.1111/j.1751-908X.2010.00036.x.

Li, X.H., Tang, G.Q., Gong, B., Yang, Y.H., Hou, K.J., Hu, Z.C., Li, Q.L., Liu, Y., and Li, W.X., 2013, Qinghu zircon: A working reference for microbeam analysis of U-Pb age and Hf and O isotopes: Chinese Science Bulletin, v. 58, p. 4647–4654, https://doi.org/10.1007/s11434-013-5932-x.

Liu, B., Han, B.F., Xu, Z., Ren, R., Zhang, J.R., Zhou, J., Su, L., and Li, Q.L., 2016, The Cambrian initiation of intra-oceanic subduction in the southern Paleo-Asian Ocean: Further evidence from the Barleik subduction-related metamorphic complex in the West Junggar region, NW China: Journal of Asian Earth Sciences, v. 123, p. 1–21, https://doi.org/10.1016/j.jseaes.2016.03.015.

Liu, Y.S., Hu, Z.C., Gao, S., Günther, D., Xu, J., Gao, C.G., and Chen, H.H., 2008, In situ analysis of major and trace elements of anhydrous minerals by LA-ICP-MS without applying an internal standard: Chemical Geology, v. 257, p. 34–43, https://doi.org/10.1016/j.chemgeo.2008.08.004.

Ludwig, K.R., 2003, User's manual for Isoplot 3.00: A geochronological toolkit for Microsoft Excel: Berkeley Geochronology Center Special Publication, v. 4, 70 p.

Ma, C., Xiao, W.J., Windley, B.F., Zhao, G.P., Han, C.M., Zhang, J.E., Luo, J., and Li, C., 2012, Tracing a subducted ridge-transform system in a late Carboniferous accretionary prism of the southern Altaids: Orthogonal sanukitoid dyke swarms in Western Junggar, NW China: Lithos, v. 140–141, p. 152–165, https://doi.org/10.1016/j.lithos.2012.02.005.

Maffione, M., and van Hinsbergen, D.J.J., 2018, Reconstructing plate boundaries in the Jurassic Neo-Tethys from the East and West Vardar ophiolites (Greece and Serbia): Tectonics, v. 37, p. 858–887, https://doi.org/10.1002/2017TC004790.

Martin, H., Smithies, R., Rapp, R., Moyen, J.F., and Champion, D., 2005, An overview of adakite, tonalite–trondhjemite–granodiorite (TTG), and sanukitoid: Relationships and some implications for crustal evolution: Lithos, v. 79, p. 1–24, https://doi.org/10.1016/j.lithos.2004.04.048.

Maunder, B., Prytulak, J., Goes, S., and Reagan, M., 2020, Rapid subduction initiation and magmatism in the Western Pacific driven by internal vertical forces: Nature Communications, v. 11, p. 1874, https://doi.org/10.1038/s41467-020-15737-4.

Meert, J., 2003, A synopsis of events related to the assembly of eastern Gondwana: Tectonophysics, v. 362, p. 1–40, https://doi.org/10.1016/S0040-1951(02)00629-7.

Merdith, A.S., Williams, S.E., Collins, A.S., Tetley, M.G., Mulder, J.A., Blades, M.L., Young, A., Armistead, S.E., Cannon, J., Zahirovic, S., and Müller, R.D., 2021, Extending full-plate tectonic models into deep time: Linking the Neoproterozoic and the Phanerozoic: Earth-Science Reviews, v. 214, https://doi.org/10.1016/j.earscirev.2020.103477.

Metcalf, R.V., and Shervais, J.W., 2008, Suprasubduction-zone ophiolites: Is there really an ophiolite conundrum?, *in* Wright, J.E., and Shervais, J.W., eds., Ophiolites, Arcs, and Batholiths: A Tribute to Cliff Hopson: Geological Society of America Special Paper, v. 438, p. 191–222.

Morag, N., Golan, T., Katzir, Y., Coble, M.A., Kitajima, K., and Valley, J.W., 2020, The origin of plagiogranites: Coupled SIMS O isotope ratios, U-Pb dating and trace element composition of zircon from the Troodos Ophiolite, Cyprus: Journal of Petrology, v. 61, no. 5, https://doi.org/10.1093/petrology/egaa057.

Moyen, J.F., 2009, High Sr/Y and La/Yb ratios: The meaning of the "adakitic signature": Lithos, v. 112, p. 556–574, https://doi.org/10.1016/j.lithos.2009.04.001.

Pearce, J.A., 2008, Geochemical fingerprinting of oceanic basalts with applications to ophiolite classification and the search for Archean oceanic crust: Lithos, v. 100, p. 14–48, https://doi.org/10.1016/j.lithos.2007.06.016.

Reagan, M.K., Ishizuka, O., Stern, R.J., Kelley, K.A., Ohara, Y., Blichert-Toft, J., Bloomer, S.H., Cash, J., Fryer, P., Hanan, B., Hickey-Vargas, R., Ishii, T., Kimura, J.I., Peate, D.W., Rowe, M.C., and Woods, M., 2010, Fore-arc basalts and subduction initiation in the Izu-Bonin-Mariana system: Geochemistry, Geophysics, Geosystems, v. 11, p. 1–17, https://doi.org/10.1029/2009GC002871.

Reagan, M.K., McClelland, W.C., Girard, G., Goff, K.R., Peate, D.W., Ohara, Y., and Stern, R.J., 2013, The geology of the southern Mariana fore-arc crust: Implications for the scale of Eocene volcanism in the western Pacific: Earth and Planetary Science Letters, v. 380, p. 41–51, https://doi.org/10.1016/j.epsl.2013.08.013.

Ren, R., Han, B.F., Xu, Z., Zhou, Y.Z., Liu, B., Zhang, L., Chen, J.F., Su, L., Li, J., Li, X.H., and Li, Q.L., 2014, When did the subduction first initiate in the southern Paleo-Asian Ocean: New constraints from a Cambrian intra-oceanic arc system in West Junggar, NW China: Earth and Planetary Science Letters, v. 388, p. 222–236, https://doi.org/10.1016/j.epsl.2013.11.055.

Safonova, I., Kotlyarov, A., Krivonogov, S., and Xiao, W.J., 2017, Intra-oceanic arcs of the Paleo-Asian Ocean: Gondwana Research, v. 50, p. 167–194, https://doi.org/10.1016/j.gr.2017.04.005.

Şengör, A.M.C., Natal'in, B.A., and Burtman, V.S., 1993, Evolution of the Altaid tectonic collage and Palaeozoic crustal growth in Eurasia: Nature, v. 364, p. 299–307, https://doi.org/10.1038/364299a0.

Shen, P., Pan, H., Seitmuratova, E., Yuan, F., and Jakupova, S., 2015, A Cambrian intraoceanic subduction system in the Bozshakol area, Kazakhstan: Lithos, v. 224–225, p. 61–77, https://doi.org/10.1016/j.lithos.2015.02.025.

Shimoda, G., Tatsumi, Y., Nohda, S., Ishizaka, K., and Jahn, B.M., 1998, Setouchi high-Mg andesites revisited: Geochemical evidence for melting of subducted sediments: Earth and Planetary Science Letters, v. 160, p. 479–492, https://doi.org/10.1016/S0012-821X(98)00105-8.

Söderlund, U., Patchett, P.J., Vervoort, J.D., and Isachsen, C.E., 2004, The ^{176}Lu decay constant determined by

Lu-Hf and U-Pb isotope systematics of Precambrian mafic intrusions: Earth and Planetary Science Letters, v. 219, p. 311–324, https://doi.org/10.1016/S0012-821X(04)00012-3.

Stern, R.J., 2002, Subduction zones: Reviews of Geophysics, v. 40, p. 1–40, https://doi.org/10.1029/2001RG000108.

Stern, R.J., 2004, Subduction initiation: Spontaneous and induced: Earth and Planetary Science Letters, v. 226, p. 275–292, https://doi.org/10.1016/S0012-821X(04)00498-4.

Stern, R.J., and Gerya, T., 2018, Subduction initiation in nature and models: A review: Tectonophysics, v. 746, p. 173–198, https://doi.org/10.1016/j.tecto.2017.10.014.

Sun, S.S., and McDonough, W.F., 1989, Chemical and isotopic systematics of ocean basalt: Implications for mantle composition and processes, *in* Saunders, A.D., and Norry, M.J., eds., Magmatism in the Ocean Basins: Geological Society of London, Special Publications, v. 42, p. 313–345, https://doi.org/10.1144/GSL.SP.1989.042.01.19.

Tang, G.J., Wang, Q., Wyman, D.A., and Dan, W., 2019, Crustal maturation through chemical weathering and crustal recycling revealed by Hf-O-B isotopes: Earth and Planetary Science Letters, v. 524, https://doi.org/10.1016/j.epsl.2019.115709.

Ulvrova, M.M., Coltice, N., Williams, S., and Tackley, P.J., 2019a, Where does subduction initiate and cease? A global scale perspective: Earth and Planetary Science Letters, v. 528, https://doi.org/10.1016/j.epsl.2019.115836.

Ulvrova, M.M., Brune, S., and Williams, S., 2019b, Breakup without borders: How continents speed up and slow down during rifting: Geophysical Research Letters, v. 46, p. 1338–1347, https://doi.org/10.1029/2018GL080387.

Valley, J.W., Kinny, P.D., Schulze, D.J., and Spicuzza, M.J., 1998, Zircon megacrysts from kimberlite: Oxygen isotope variability among mantle melts: Contributions to Mineralogy and Petrology, v. 133, p. 1–11, https://doi.org/10.1007/s004100050432.

Van der Voo, R., Levashova, N.M., Skrinnik, L.I., Kara, T.V., and Bazhenov, M.L., 2006, Late orogenic, large-scale rotations in the Tien Shan and adjacent mobile belts in Kyrgyzstan and Kazakhstan: Tectonophysics, v. 426, p. 335–360, https://doi.org/10.1016/j.tecto.2006.08.008.

Vervoort, J.D., Patchett, P.J., Soderlund, U., and Baker, M., 2004, Isotopic composition of Yb and the determination of Lu concentrations and Lu/Hf ratios by isotope dilution MC-ICP-MS: Geochemistry, Geophysics, Geosystems, v. 5, no. 11, https://doi.org/10.1029/2004GC000721.

Wan, B., Li, S.H., Xiao, W.J., and Windley, B.F., 2018, Where and when did the Paleo-Asian ocean form?: Precambrian Research, v. 317, p. 241–252, https://doi.org/10.1016/j.precamres.2018.09.003.

Whattam, S.A., and Stern, R.J., 2011, The 'subduction initiation rule': A key for linking ophiolites, intra-oceanic forearcs, and subduction initiation: Contributions to Mineralogy and Petrology, v. 162, p. 1031–1045, https://doi.org/10.1007/s00410-011-0638-z.

Whattam, S.A., Gazel, E., Yi, K., and Denyer, P., 2016, Origin of plagiogranites in oceanic complexes: A case study of the Nicoya and Santa Elena terranes, Costa Rica: Lithos, v. 262, p. 75–87, https://doi.org/10.1016/j.lithos.2016.06.017.

Wilhem, C., Windley, B.F., and Stampfli, G.M., 2012, The Altaids of Central Asia: A tectonic and evolutionary innovative review: Earth-Science Reviews, v. 113, p. 303–341, https://doi.org/10.1016/j.earscirev.2012.04.001.

Windley, B.F., Alexeiev, D., Xiao, W.J., Kröner, A., and Badarch, G., 2007, Tectonic models for accretion of the Central Asian Orogenic Belt: Journal of the Geological Society, v. 164, p. 31–47, https://doi.org/10.1144/0016-76492006-022.

Woodhead, J.D., Hergt, J.M., Davidson, J.P., and Eggins, S.M., 2001, Hafnium isotope evidence for 'conservative' element mobility during subduction zone processes: Earth and Planetary Science Letters, v. 192, p. 331–346, https://doi.org/10.1016/S0012-821X(01)00453-8.

Wu, F.Y., Wan, B., Zhao, L., Xiao, W.J., and Zhu, R.X., 2020, Tethyan geodynamics: Yanshi Xuebao, v. 36, p. 1627–1674.

Xia, X.P., Sun, M., Geng, H.Y., Sun, Y.L., Wang, Y.J., and Zhao, G.C., 2011, Quasi-simultaneous determination of U-Pb and Hf isotope compositions of zircon by excimer laser-ablation multiple-collector ICPMS: Journal of Analytical Atomic Spectrometry, v. 26, p. 1868–1871, https://doi.org/10.1039/c1ja10116a.

Xiao, W.J., and Santosh, M., 2014, The western Central Asian Orogenic Belt: A window to accretionary orogenesis and continental growth: Gondwana Research, v. 25, p. 1429–1444, https://doi.org/10.1016/j.gr.2014.01.008.

Xiao, W.J., Windley, B., Sun, S., Li, J.L., Huang, B.C., Han, C.M., Yuan, C., Sun, M., and Chen, H.L., 2015, A tale of amalgamation of three Permo-Triassic collage systems in Central Asia: Oroclines, sutures, and terminal accretion: Annual Review of Earth and Planetary Sciences, v. 43, p. 477–507, https://doi.org/10.1146/annurev-earth-060614-105254.

Xu, Z., Han, B.F., Ren, R., Zhou, Y.Z., Zhang, L., Chen, J.F., Su, L., Li, X.H., and Liu, D.Y., 2012, Ultramafic–mafic mélange, island arc and post-collisional intrusions in the Mayile Mountain, West Junggar, China: Implications for Paleozoic intra-oceanic subduction–accretion process: Lithos, v. 132, p. 141–161, https://doi.org/10.1016/j.lithos.2011.11.016.

Xu, Z., Han, B.F., Ren, R., Zhou, Y.Z., and Su, L., 2013, Palaeozoic multiphase magmatism at Barleik Mountain, southern West Junggar, Northwest China: Implications for tectonic evolution of the West Junggar: International Geology Review, v. 55, p. 633–656, https://doi.org/10.1080/00206814.2012.741315.

Yang, Q., Xia, X.P., Zhang, W.F., Zhang, Y.Q., Xiong, B.Q., Xu, Y.G., Wang, Q., and Wei, G.J., 2018, An evaluation of precision and accuracy of SIMS oxygen isotope analysis: Solid Earth Sciences, v. 3, p. 81–86, https://doi.org/10.1016/j.sesci.2018.05.001.

Yao, J.L., Cawood, P.A., Zhao, G.C., Han, Y.G., Xia, X.P., Liu, Q., and Wang, P., 2021, Mariana-type ophiolites constrain the establishment of modern plate tectonic regime during Gondwana assembly: Nature Communications, v. 12, no. 4189, https://doi.org/10.1038/s41467-021-24422-z.

Yin, J.Y., Long, X.P., Yuan, C., Sun, M., Zhao, G.C., and Geng, H.Y., 2013, A Late Carboniferous–Permian slab window in the West Junggar of NW China: Geochronological and geochemical evidence from mafic to intermediate dikes: Lithos, v. 175–176, p. 146–162, https://doi.org/10.1016/j.lithos.2013.04.005.

Yu, M.M., Dilek, Y., Yumul, G.P., Jr., Yan, Y., Dimalanta, C.B., and Huang, C.Y., 2020, Slab-controlled elemental–isotopic enrichments during subduction initiation magmatism and variations in forearc chemostratigraphy: Earth and Planetary Science Letters, v. 538, https://doi.org/10.1016/j.epsl.2020.116217.

Zhang, J.E., Xiao, W.J., Luo, J., Chen, Y.C., Windley, B.F., Song, D.F., Han, C.M., and Safonova, I., 2018a, Collision of the Tacheng block with the Mayile-Barleik-Tangbale accretionary complex in Western Junggar, NW China: Implication for Early-Middle Paleozoic architecture of the western Altaids: Journal of Asian Earth Sciences, v. 159, p. 259–278, https://doi.org/10.1016/j.jseaes.2017.03.023.

Zhang, Y.Y., Sun, M., Yuan, C., Long, X.P., Jiang, Y.D., Li, P.F., Huang, Z.Y., and Du, L., 2018b, Alternating trench advance and retreat: Insights from Paleozoic magmatism in the eastern Tianshan, Central Asian Orogenic Belt: Tectonics, v. 37, p. 2142–2164, https://doi.org/10.1029/2018TC005051.

Zhao, G.C., Wang, Y.J., Huang, B.C., Dong, Y.P., Li, S.Z., Zhang, G.W., and Yu, S., 2018, Geological reconstructions of the East Asian blocks: From the breakup of Rodinia to the assembly of Pangea: Earth-Science Reviews, v. 186, p. 262–286, https://doi.org/10.1016/j.earscirev.2018.10.003.

Science Editor: Brad S. Singer
Associate Editor: Haibo Zou

Manuscript Received 22 August 2021
Revised Manuscript Received 13 December 2021
Manuscript Accepted 23 January 2022

Printed in the USA